Study and use of spectral symbol properties for isogeometric matrices on trimmed geometries

Study and use of spectral symbol properties for isogeometric matrices on trimmed geometries

Carlo Garoni[a,*], Carla Manni[a], Francesca Pelosi[b], Hendrik Speleers[a]

[a] *Department of Mathematics, University of Rome Tor Vergata, Via della Ricerca Scientifica 1, 00133, Rome, Italy*
[b] *Department of Information Engineering and Mathematical Sciences, University of Siena, Via Roma 56, 53100, Siena, Italy*

Abstract

We study the spectral behavior of (sequences of) matrices resulting from immersed isogeometric discretizations on trimmed geometries. They enjoy an asymptotic spectral distribution, described by a (spectral) symbol, and we discuss some properties of this symbol. In particular, we show that the structure and properties of the symbol are completely analogous to the untrimmed case when a suitable natural restriction of the parametric domain is considered. This spectral knowledge can be exploited to identify potentially fast preconditioners for the considered immersed discretization matrices and we propose a specific CG preconditioner based on the symbol. We also provide numerical experiments that support the correctness of the theoretical results and illustrate the performance of the proposed preconditioner.

Keywords: Isogeometric analysis, Immersed methods, Trimmed geometries, Cardinal B-splines

1. Introduction

An important step for the development of mathematical models governing physical phenomena and the reliability and efficiency of their numerical treatment is a proper representation of the physical domains of interest at different levels of refinement. In computer-aided design (CAD) models, a physical domain is usually represented by one or more boundary surfaces, described by suitable geometry maps over a parametric domain. Trimming is a popular procedure in CAD: it is used to define visible areas over surfaces independent of the underlying parametric space and consequently it allows for a simple representation of surfaces with non-rectangular structure.

Dealing with trimmed geometries is one of the current challenges both in CAD and isogeometric analysis (IgA), a powerful paradigm that aims to close the gap between design and analysis by performing numerical simulations based on CAD technologies [6, 24]. Borrowing the CAD philosophy, in the classical IgA approach the physical domain is described by a geometry map defined over a parametric domain (usually possessing an elementary rectangular structure) and most often expressed in terms of polynomial B-splines or their rational extensions called NURBS. The unknown fields are then approximated by means of the same primitives (composed with the inverse of the geometry map); see [6]. When dealing with trimmed geometries, the trimmed part of the parametric domain has to be taken into account. In this perspective, coupling the isogeometric paradigm with the framework of so-called immersed boundary methods — also known as immersed interface, fictitious domain, or embedded domain methods [21, 27] — emerges as a natural choice. According to the philosophy of immersed boundary methods, the trimmed parametric domain is embedded in a tensor-product mesh and simple, mesh-aligned numerical schemes can be applied. Clearly, immersed methods need to treat the mesh elements that are cut by the trimming curves with some special, and often ad-hoc, techniques to achieve acceptably accurate results.

The efficiency and accuracy of a numerical simulation process are the result of a synergistic interaction between different players. Among the others, fast and robust (iterative) solvers for the resulting linear systems are of importance. In this perspective, knowledge about the spectral behavior of the involved discretization matrices is very helpful. Such knowledge for matrices arising from various IgA discretizations with boundary conditions in strong form was investigated in a sequence of papers; we refer the reader to [13] and references therein.

*Corresponding author
Email addresses: garoni@mat.uniroma2.it (Carlo Garoni), manni@mat.uniroma2.it (Carla Manni), francesca.pelosi@unisi.it (Francesca Pelosi), speleers@mat.uniroma2.it (Hendrik Speleers)

The spectral behavior of matrices resulting from immersed isogeometric methods based on spline spaces of maximal smoothness, with Dirichlet boundary conditions imposed in a weak form [1, 25], was recently analyzed in [10] for general variable-coefficient Poisson problems. In particular, by exploiting the theory of reduced generalized locally Toeplitz (GLT) sequences [2, 26], it was shown that immersed B-spline discretization matrices enjoy an asymptotic spectral distribution when the matrix size tends to infinity. This asymptotic distribution can be compactly described by a function called (spectral) symbol. The symbol does not depend on the method used to impose the boundary conditions but it incorporates the discretization technique and the diffusion coefficients of the differential problem.

In this paper, we deepen the spectral analysis for immersed isogeometric methods presented in [10] focusing on domains obtained by a trimmed geometry map. More specifically, we study the corresponding spectral symbol and we prove that its structure and properties are completely analogous to the untrimmed case: we only need to replace the standard full parametric domain $[0,1]^d$ by $\boldsymbol{G}^{-1}(\Omega)$, where $\boldsymbol{G}$ is the trimmed geometry map and Ω the physical domain; see Theorem 4.4. We also illustrate how this knowledge can be exploited to identify potentially fast preconditioners for the linear systems arising from the considered immersed isogeometric discretizations. Based on the symbol, we propose a specific CG preconditioner and we test its performance.

The paper is organized as follows. Section 2 summarizes some notation and basic definitions that will be used in the paper. In Section 3 we describe our model problem and the considered Galerkin discretization with the adopted weak imposition of boundary conditions. Moreover, we outline some properties of tensor-product cardinal B-splines, which are the functions employed in our discretization, and we briefly discuss the strategy we apply to modify the basis functions that have tiny overlaps with the trimmed domain in order to improve the conditioning. In Section 4 we show that the resulting discretization matrices enjoy an asymptotic spectral distribution described by a symbol and we study the properties of this symbol. We also propose a specific CG preconditioner based on the symbol. Section 5 presents some numerical experiments to validate the obtained theoretical results and to illustrate the performance of the proposed preconditioner. Finally, in Section 6 we end with some concluding remarks.

2. Preliminaries

In this section we collect some preliminaries on multi-index notation and spectral analysis tools.

2.1. Multi-index notation

A multi-index $\boldsymbol{i}$ of size d, also called a d-index, is a (row) vector in $\mathbb{Z}^d$; its components are denoted by $i_1,\dots,i_d$. We indicate by $\mathbf{0}$ and $\mathbf{1}$ the vectors of all zeros and all ones, respectively (their size will be clear from the context). For any $\boldsymbol{h}\in\mathbb{R}^d$, we set $N(\boldsymbol{h})=\prod_{j=1}^d h_j$. If $\boldsymbol{h},\boldsymbol{k}\in\mathbb{R}^d$, an inequality such as $\boldsymbol{h}\le\boldsymbol{k}$ means that $h_j\le k_j$ for all $j=1,\dots,d$. If $\boldsymbol{h},\boldsymbol{k}$ are d-indices such that $\boldsymbol{h}\le\boldsymbol{k}$, the d-index range $\{\boldsymbol{h},\dots,\boldsymbol{k}\}$ is the set $\{\boldsymbol{i}\in\mathbb{Z}^d:\boldsymbol{h}\le\boldsymbol{i}\le\boldsymbol{k}\}$. We assume for this set the standard lexicographic ordering:

$$\Big[\ \dots\ \Big[\ [\ (i_1,\dots,i_d)\ ]_{i_d=h_d,\dots,k_d}\ \Big]_{i_{d-1}=h_{d-1},\dots,k_{d-1}}\ \dots\ \Big]_{i_1=h_1,\dots,k_1}.$$

For instance, in the case $d=2$ the ordering is

$$\begin{aligned}&(h_1,h_2),\ (h_1,h_2+1),\ \dots,\ (h_1,k_2),\ (h_1+1,h_2),\ (h_1+1,h_2+1),\ \dots,\ (h_1+1,k_2),\\ &\dots\dots\dots,\ (k_1,h_2),\ (k_1,h_2+1),\ \dots,\ (k_1,k_2).\end{aligned}$$

When a d-index $\boldsymbol{i}$ varies in a finite set $\mathcal{I}\subset\mathbb{Z}^d$ (this is simply written as $\boldsymbol{i}\in\mathcal{I}$), it is understood that $\boldsymbol{i}$ follows the lexicographic ordering. Operations involving d-indices (or general vectors with d components) that have no meaning in the vector space $\mathbb{R}^d$ must always be interpreted in the componentwise sense. For instance, $\boldsymbol{n}\boldsymbol{x}=(n_1x_1,\dots,n_dx_d)$, $\boldsymbol{\nu}^2=(\nu_1^2,\dots,\nu_d^2)$, $\alpha\boldsymbol{i}/\boldsymbol{j}=(\alpha i_1/j_1,\dots,\alpha i_d/j_d)$ for all $\alpha\in\mathbb{R}$, etc. If $\boldsymbol{a},\boldsymbol{b}\in\mathbb{R}^d$ with $\boldsymbol{a}\le\boldsymbol{b}$, we denote by $(\boldsymbol{a},\boldsymbol{b})$ and $[\boldsymbol{a},\boldsymbol{b}]$ the open d-dimensional rectangle $(a_1,b_1)\times\cdots\times(a_d,b_d)$ and the closed d-dimensional rectangle $[a_1,b_1]\times\cdots\times[a_d,b_d]$, respectively.

2.2. Singular value and spectral distribution of a sequence of matrices

A sequence of matrices is a sequence of the form $\{A_n\}_n$, where n varies in some infinite subset of $\mathbb{N}$ and A_n is a square matrix of size m_n such that $m_n\to\infty$ as $n\to\infty$. Let $C_c(\mathbb{R})$ (resp., $C_c(\mathbb{C})$) be the space of continuous complex-valued functions with bounded support defined on $\mathbb{R}$ (resp., $\mathbb{C}$). If $A\in\mathbb{C}^{m\times m}$ then the singular values and eigenvalues of A are denoted by $\sigma_1(A),\dots,\sigma_m(A)$ and $\lambda_1(A),\dots,\lambda_m(A)$.

Definition 2.1. Let $\{A_n\}_n$ be a sequence of matrices, with A_n of size m_n, and let $f : D \subset \mathbb{R}^k \to \mathbb{C}$ be a measurable function defined on a set D with $0 < \mu_k(D) < \infty$.

- We say that $\{A_n\}_n$ has a spectral (or eigenvalue) distribution described by f, and we write $\{A_n\}_n \sim_\lambda f$, if

$$\lim_{n\to\infty} \frac{1}{m_n} \sum_{i=1}^{m_n} F(\lambda_i(A_n)) = \frac{1}{\mu_k(D)} \int_D F(f(\boldsymbol{x}))\mathrm{d}\boldsymbol{x}, \qquad \forall\, F \in C_c(\mathbb{C}). \tag{2.1}$$

  In this case, f is called the spectral (or eigenvalue) symbol of $\{A_n\}_n$.
- We say that $\{A_n\}_n$ has a singular value distribution described by f, and we write $\{A_n\}_n \sim_\sigma f$, if

$$\lim_{n\to\infty} \frac{1}{m_n} \sum_{i=1}^{m_n} F(\sigma_i(A_n)) = \frac{1}{\mu_k(D)} \int_D F(|f(\boldsymbol{x})|)\mathrm{d}\boldsymbol{x}, \qquad \forall\, F \in C_c(\mathbb{R}). \tag{2.2}$$

  In this case, f is called the singular value symbol of $\{A_n\}_n$.

Remark 2.1. The informal meaning behind the spectral distribution (2.1) is the following: assuming that f is continuous almost everywhere, the eigenvalues of A_n, except possibly for $o(m_n)$ outliers, are approximately equal to the samples of f over a uniform grid in the domain D (for n large enough). A completely analogous meaning can be given for the singular value distribution (2.2).

3. Immersed B-spline discretization of diffusion problems

Consider the d-dimensional diffusion problem

$$\begin{cases} -\nabla \cdot A\nabla u = \mathrm{f}, & \text{in } \Omega, \\ u = \mathrm{g}, & \text{on } \Gamma, \end{cases} \tag{3.1}$$

where Ω is an open Lipschitz domain in $\mathbb{R}^d$, $\Gamma = \partial\Omega$, $A = [a_{\alpha\beta}]_{\alpha,\beta=1}^d$ is a symmetric positive definite matrix of (variable) diffusion coefficients, and f, g are given functions. In this section we expound the immersed Galerkin method from [10] to discretize (3.1), which makes use of tensor-product (cardinal) B-splines.

3.1. Weak boundary discretization

Suppose the domain Ω is covered by a (mapped) finite element mesh. Let Ω_{in} be the union of the closed elements contained in Ω and Ω_Γ the union of the closed elements intersecting both Γ and Ω. We define $\Omega_{\Gamma,\mathrm{in}} = \Omega_\Gamma \cap \Omega$ so that $\Omega = \Omega_{\mathrm{in}} \cup \Omega_{\Gamma,\mathrm{in}}$. Following the approach in [10], we introduce an additional unknown flux $\boldsymbol{\sigma}$ and problem (3.1) can be translated into the following weak form: find $u \in H^1(\Omega)$ and $\boldsymbol{\sigma} \in (L^2(\Omega_{\Gamma,\mathrm{in}}))^d$ such that

$$\begin{cases} (A\nabla u, \nabla v)_\Omega - \langle \boldsymbol{\sigma}\cdot\boldsymbol{n}_\Gamma, v\rangle_\Gamma + \dfrac{1}{\eta}(\boldsymbol{\sigma} - A\nabla u, \nabla v)_{\Omega_{\Gamma,\mathrm{in}}} = \langle \mathrm{f}, v\rangle_\Omega, & \forall\, v \in H^1(\Omega), \\ -\dfrac{1}{\eta}(A^{-1}\boldsymbol{\sigma} - \nabla u, \boldsymbol{\tau})_{\Omega_{\Gamma,\mathrm{in}}} - \langle u, \boldsymbol{\tau}\cdot\boldsymbol{n}_\Gamma\rangle_\Gamma = -\langle \mathrm{g}, \boldsymbol{\tau}\cdot\boldsymbol{n}_\Gamma\rangle_\Gamma, & \forall\, \boldsymbol{\tau} \in (L^2(\Omega_{\Gamma,\mathrm{in}}))^d, \end{cases}$$

where η is a free a priori fixed parameter, $\boldsymbol{n}_\Gamma$ is the outward unit normal to Γ, and the symbols $\langle\cdot,\cdot\rangle_E$ and $(\cdot,\cdot)_E$ denote the L^2 inner products for scalar and vector functions over E, respectively:

$$\langle \alpha, \beta\rangle_E = \int_E \alpha\beta, \qquad \alpha, \beta \in L^2(E),$$
$$(\boldsymbol{\alpha}, \boldsymbol{\beta})_E = \int_E \boldsymbol{\alpha}\cdot\boldsymbol{\beta}, \qquad \boldsymbol{\alpha}, \boldsymbol{\beta} \in (L^2(E))^d.$$

We choose two finite dimensional vector spaces $\mathbb{V} \subset H^1(\Omega)$ and $\mathbb{W} \subset (L^2(\Omega_{\Gamma,\mathrm{in}}))^d$, and we look for an approximation $u_\mathbb{V}$ of u by solving the following discrete problem: find $u_\mathbb{V} \in \mathbb{V}$ and $\boldsymbol{\sigma}_\mathbb{W} \in \mathbb{W}$ such that

$$\begin{cases} (A\nabla u_\mathbb{V}, \nabla v_\mathbb{V})_\Omega - \langle \boldsymbol{\sigma}_\mathbb{W}\cdot\boldsymbol{n}_\Gamma, v_\mathbb{V}\rangle_\Gamma + \dfrac{1}{\eta}(\boldsymbol{\sigma}_\mathbb{W} - A\nabla u_\mathbb{V}, \nabla v_\mathbb{V})_{\Omega_{\Gamma,\mathrm{in}}} = \langle \mathrm{f}, v_\mathbb{V}\rangle_\Omega, & \forall\, v_\mathbb{V} \in \mathbb{V}, \\ -\dfrac{1}{\eta}(A^{-1}\boldsymbol{\sigma}_\mathbb{W} - \nabla u_\mathbb{V}, \boldsymbol{\tau}_\mathbb{W})_{\Omega_{\Gamma,\mathrm{in}}} - \langle u_\mathbb{V}, \boldsymbol{\tau}_\mathbb{W}\cdot\boldsymbol{n}_\Gamma\rangle_\Gamma = -\langle \mathrm{g}, \boldsymbol{\tau}_\mathbb{W}\cdot\boldsymbol{n}_\Gamma\rangle_\Gamma, & \forall\, \boldsymbol{\tau}_\mathbb{W} \in \mathbb{W}. \end{cases} \tag{3.2}$$

Table 3.1: Schematic representation of the blocks involved in the linear systems (3.3) and (3.4).

$(A\nabla u_{\mathbb{V}}, \nabla v_{\mathbb{V}})_{\Omega}$	$\longrightarrow$	$K^{uu}\boldsymbol{U}$	$\longrightarrow$	$K^{uu} = \Big[(A\nabla\varphi_j, \nabla\varphi_i)_{\Omega}\Big]_{i,j=1}^{N}$
$-\frac{1}{\eta}(A\nabla u_{\mathbb{V}}, \nabla v_{\mathbb{V}})_{\Omega_{\Gamma,\mathrm{in}}}$	$\longrightarrow$	$K^{uu}_{\mathrm{in}}\boldsymbol{U}$	$\longrightarrow$	$K^{uu}_{\mathrm{in}} = -\frac{1}{\eta}\Big[(A\nabla\varphi_j, \nabla\varphi_i)_{\Omega_{\Gamma,\mathrm{in}}}\Big]_{i,j=1}^{N}$
$-\frac{1}{\eta}(A^{-1}\boldsymbol{\sigma}_{\mathbb{W}}, \boldsymbol{\tau}_{\mathbb{W}})_{\Omega_{\Gamma,\mathrm{in}}}$	$\longrightarrow$	$K^{\sigma\sigma}\boldsymbol{\Sigma}$	$\longrightarrow$	$K^{\sigma\sigma} = -\frac{1}{\eta}\Big[(A^{-1}\boldsymbol{\psi}_s, \boldsymbol{\psi}_r)_{\Omega_{\Gamma,\mathrm{in}}}\Big]_{r,s=1}^{L}$
$\frac{1}{\eta}(\boldsymbol{\sigma}_{\mathbb{W}}, \nabla v_{\mathbb{V}})_{\Omega_{\Gamma,\mathrm{in}}}$	$\longrightarrow$	$K^{u\sigma}\boldsymbol{\Sigma}$	$\longrightarrow$	$K^{u\sigma} = \frac{1}{\eta}\Big[(\boldsymbol{\psi}_s, \nabla\varphi_i)_{\Omega_{\Gamma,\mathrm{in}}}\Big]_{\substack{i=1,\dots,N\\ s=1,\dots,L}}$
$\frac{1}{\eta}(\nabla u_{\mathbb{V}}, \boldsymbol{\tau}_{\mathbb{W}})_{\Omega_{\Gamma,\mathrm{in}}}$	$\longrightarrow$	$K^{\sigma u}\boldsymbol{U}$	$\longrightarrow$	$K^{\sigma u} = \frac{1}{\eta}\Big[(\nabla\varphi_j, \boldsymbol{\psi}_r)_{\Omega_{\Gamma,\mathrm{in}}}\Big]_{\substack{r=1,\dots,L\\ j=1,\dots,N}}$
$-\langle\boldsymbol{\sigma}_{\mathbb{W}}\cdot\boldsymbol{n}_{\Gamma}, v_{\mathbb{V}}\rangle_{\Gamma}$	$\longrightarrow$	$G^{u\sigma}\boldsymbol{\Sigma}$	$\longrightarrow$	$G^{u\sigma} = \Big[-\langle\boldsymbol{\psi}_s\cdot\boldsymbol{n}_{\Gamma}, \varphi_i\rangle_{\Gamma}\Big]_{\substack{i=1,\dots,N\\ s=1,\dots,L}}$
$-\langle u_{\mathbb{V}}, \boldsymbol{\tau}_{\mathbb{W}}\cdot\boldsymbol{n}_{\Gamma}\rangle_{\Gamma}$	$\longrightarrow$	$G^{\sigma u}\boldsymbol{U}$	$\longrightarrow$	$G^{\sigma u} = \Big[-\langle\varphi_j, \boldsymbol{\psi}_r\cdot\boldsymbol{n}_{\Gamma}\rangle_{\Gamma}\Big]_{\substack{r=1,\dots,L\\ j=1,\dots,N}}$
$\langle \mathrm{f}, v_{\mathbb{V}}\rangle_{\Omega}$	$\longrightarrow$	$\boldsymbol{f}$	$\longrightarrow$	$\boldsymbol{f} = \big[\langle \mathrm{f}, \varphi_i\rangle_{\Omega}\big]_{i=1}^{N}$
$-\langle \mathrm{g}, \boldsymbol{\tau}_{\mathbb{W}}\cdot\boldsymbol{n}_{\Gamma}\rangle_{\Gamma}$	$\longrightarrow$	$\boldsymbol{g}$	$\longrightarrow$	$\boldsymbol{g} = \big[-\langle \mathrm{g}, \boldsymbol{\psi}_r\cdot\boldsymbol{n}_{\Gamma}\rangle_{\Gamma}\big]_{r=1}^{L}$

In the case where $A = kI_d$, with $k > 0$ and I_d being the $d \times d$ identity matrix, it was proved in [1] that the discrete problem (3.2) is stable for $\eta > 1$ and the model is not sensitive to the choice of η. For that reason, the model is essentially free of user-defined parameters. In the numerical experiments the value is fixed to $\eta = 2$ for all the tests.

If $\boldsymbol{U}$ and $\boldsymbol{\Sigma}$ are, respectively, the coefficient vectors of $u_{\mathbb{V}}$ and $\boldsymbol{\sigma}_{\mathbb{W}}$ with respect to a fixed basis $\{\varphi_1, \dots, \varphi_N\}$ in $\mathbb{V}$ and a fixed basis $\{\boldsymbol{\psi}_1, \dots, \boldsymbol{\psi}_L\}$ in $\mathbb{W}$, then solving (3.2) is equivalent to solving the linear system

$$\begin{bmatrix} K^{uu} + K^{uu}_{\mathrm{in}} & K^{u\sigma} + G^{u\sigma} \\ K^{\sigma u} + G^{\sigma u} & K^{\sigma\sigma} \end{bmatrix} \begin{bmatrix} \boldsymbol{U} \\ \boldsymbol{\Sigma} \end{bmatrix} = \begin{bmatrix} \boldsymbol{f} \\ \boldsymbol{g} \end{bmatrix}, \tag{3.3}$$

where the meaning of the different blocks is summarized in Table 3.1. When writing the flux $\boldsymbol{\Sigma} = (K^{\sigma\sigma})^{-1}(-(K^{\sigma u} + G^{\sigma u})\boldsymbol{U} + \boldsymbol{g})$, the problem can be formulated in terms of the original unknown $\boldsymbol{U}$ only:

$$\big[K^{uu} + K^{uu}_{\mathrm{in}} - (K^{u\sigma} + G^{u\sigma})(K^{\sigma\sigma})^{-1}(K^{\sigma u} + G^{\sigma u})\big]\boldsymbol{U} = \boldsymbol{f} - (K^{u\sigma} + G^{u\sigma})(K^{\sigma\sigma})^{-1}\boldsymbol{g}. \tag{3.4}$$

Remark 3.1. Since the matrix A is supposed to be symmetric, it is easy to see that $K^{uu} = (K^{uu})^T$, $K^{uu}_{\mathrm{in}} = (K^{uu}_{\mathrm{in}})^T$, $K^{\sigma\sigma} = (K^{\sigma\sigma})^T$, $K^{\sigma u} = (K^{u\sigma})^T$ and $G^{\sigma u} = (G^{u\sigma})^T$. It follows that the matrices in (3.3) and (3.4) are symmetric.

3.2. Immersed B-spline discretization

We now briefly review the basics of the theory of tensor-product cardinal B-splines, which play a central role in our discretizations of (3.1). Let $M_p : \mathbb{R} \to \mathbb{R}$ be the cardinal B-spline of degree $p \geq 0$, defined recursively over the uniform knot sequence $\{0, 1, \dots, p+1\}$ as follows [5, 22]:

$$M_0(x) = \begin{cases} 1, & \text{if } x \in [0, 1), \\ 0, & \text{otherwise,} \end{cases}$$

$$M_p(x) = \frac{x}{p} M_{p-1}(x) + \frac{p+1-x}{p} M_{p-1}(x-1), \qquad p \geq 1.$$

Given a d-index $\boldsymbol{p} \geq \boldsymbol{0}$, the tensor-product cardinal B-spline $M_{\boldsymbol{p}} : \mathbb{R}^d \to \mathbb{R}$ is defined by

$$M_{\boldsymbol{p}}(\boldsymbol{x}) = \prod_{i=1}^{d} M_{p_i}(x_i).$$

The next proposition collects a few properties of tensor-product cardinal B-splines that follow from analogous properties of (univariate) cardinal B-splines [5, 22]. Throughout this paper, we denote by Δ_d the tensor-product mesh in $\mathbb{R}^d$ formed by the closed d-dimensional squares of side 1 with vertices taken from the integer lattice $\mathbb{Z}^d$. Each of the d-dimensional squares is referred to as an element of Δ_d.

Proposition 3.1. *Tensor-product cardinal B-splines have the following properties.*

- *Smoothness:* $M_{\boldsymbol{p}} \in C^{\min(\boldsymbol{p})-1}(\mathbb{R}^d)$.
- *Piecewise polynomial structure:* $M_{\boldsymbol{p}}$ *is a* d*-variate piecewise polynomial of total degree* $\sum_{j=1}^{d} p_j$ *over the tensor-product mesh* Δ_d.
- *Positivity and support:* $M_{\boldsymbol{p}} > 0$ *over* $(\boldsymbol{0}, \boldsymbol{p}+\boldsymbol{1})$ *and* $\operatorname{supp}(M_{\boldsymbol{p}}) = [\boldsymbol{0}, \boldsymbol{p}+\boldsymbol{1}]$.
- *Symmetry:* $M_{\boldsymbol{p}}(\frac{\boldsymbol{p}+\boldsymbol{1}}{2} + \boldsymbol{x}) = M_{\boldsymbol{p}}(\frac{\boldsymbol{p}+\boldsymbol{1}}{2} - \boldsymbol{x})$ *for* $\boldsymbol{x} \in \mathbb{R}^d$.
- L^2 *inner product of derivatives: for* $\boldsymbol{p}, \boldsymbol{q} \geq \boldsymbol{1}$ *and* $\alpha, \beta = 1, \ldots, d$,

$$\int_{\mathbb{R}^d} \frac{\partial M_{\boldsymbol{p}}}{\partial x_\alpha}(\boldsymbol{x}) \frac{\partial M_{\boldsymbol{q}}}{\partial x_\beta}(\boldsymbol{x}+\boldsymbol{y}) \mathrm{d}\boldsymbol{x} = -\frac{\partial^2 M_{\boldsymbol{p}+\boldsymbol{q}+\boldsymbol{1}}}{\partial x_\alpha \partial x_\beta}(\boldsymbol{p}+\boldsymbol{1}+\boldsymbol{y}) = -\frac{\partial^2 M_{\boldsymbol{p}+\boldsymbol{q}+\boldsymbol{1}}}{\partial x_\alpha \partial x_\beta}(\boldsymbol{q}+\boldsymbol{1}-\boldsymbol{y}), \qquad \boldsymbol{y} \in \mathbb{R}^d.$$

- *Partition of unity:* $\sum_{\boldsymbol{i} \in \mathbb{Z}^d} M_{\boldsymbol{p}}(\boldsymbol{x} - \boldsymbol{i}) = 1$ *for* $\boldsymbol{x} \in \mathbb{R}^d$.
- *Local linear independence: the functions* $M_{\boldsymbol{p}}(\cdot - \boldsymbol{i})$, $\boldsymbol{i} \in \mathbb{Z}^d$ *are locally linearly independent.*

Given a d-index $\boldsymbol{n} \geq \boldsymbol{1}$, the corresponding scaled integer translates of tensor-product cardinal B-splines are defined by

$$M_{\boldsymbol{n},\boldsymbol{p},\boldsymbol{i}}(\boldsymbol{x}) = M_{\boldsymbol{p}}(\boldsymbol{n}\boldsymbol{x} - \boldsymbol{i}), \qquad \boldsymbol{i} \in \mathbb{Z}^d.$$

These functions are d-variate piecewise polynomials over the scaled mesh $\frac{\boldsymbol{1}}{\boldsymbol{n}}\Delta_d$ consisting of the scaled elements $\frac{\boldsymbol{1}}{\boldsymbol{n}}E = \{\frac{\boldsymbol{1}}{\boldsymbol{n}}\boldsymbol{x} : \boldsymbol{x} \in E\}$, where E is an element of Δ_d.

We are now ready to detail the spaces $\mathbb{V}$ and $\mathbb{W}$ based on mapped tensor-product cardinal B-splines. Given an invertible geometry map $\boldsymbol{G}$ from a subset $\hat{\Omega}$ of $[0,1]^d$ to $\overline{\Omega}$, we define the mapped basis functions $M^{\boldsymbol{G}}_{\boldsymbol{n},\boldsymbol{p},\boldsymbol{i}} : \overline{\Omega} \to \mathbb{R}$,

$$M^{\boldsymbol{G}}_{\boldsymbol{n},\boldsymbol{p},\boldsymbol{i}}(\boldsymbol{x}) = M_{\boldsymbol{n},\boldsymbol{p},\boldsymbol{i}}(\boldsymbol{G}^{-1}(\boldsymbol{x})), \qquad \boldsymbol{i} \in \mathbb{Z}^d. \tag{3.5}$$

The spaces $\mathbb{V}$ and $\mathbb{W}$ are defined as follows:

$$\begin{aligned}
\mathbb{V} &= \langle M^{\boldsymbol{G}}_{\boldsymbol{n},\boldsymbol{p},\boldsymbol{i}} : \boldsymbol{i} \in \mathcal{I}_{\boldsymbol{n},\boldsymbol{p}} \rangle, & \mathcal{I}_{\boldsymbol{n},\boldsymbol{p}} &= \{\boldsymbol{i} \in \mathbb{Z}^d : \operatorname{supp}(M_{\boldsymbol{n},\boldsymbol{p},\boldsymbol{i}}) \cap \boldsymbol{G}^{-1}(\Omega) \neq \emptyset\}, \\
\mathbb{W} &= (\langle M^{\boldsymbol{G}}_{\boldsymbol{n},\boldsymbol{p},\boldsymbol{i}} : \boldsymbol{i} \in \mathcal{I}^{\Gamma}_{\boldsymbol{n},\boldsymbol{p}} \rangle)^d, & \mathcal{I}^{\Gamma}_{\boldsymbol{n},\boldsymbol{p}} &= \{\boldsymbol{i} \in \mathbb{Z}^d : \operatorname{supp}(M_{\boldsymbol{n},\boldsymbol{p},\boldsymbol{i}}) \cap \boldsymbol{G}^{-1}(\mathring{\Omega}_{\Gamma,\mathrm{in}}) \neq \emptyset\},
\end{aligned}$$

where we assume that the domain of each $M^{\boldsymbol{G}}_{\boldsymbol{n},\boldsymbol{p},\boldsymbol{i}}$ is restricted to Ω in the definition of $\mathbb{V}$ and to $\Omega_{\Gamma,\mathrm{in}}$ in the definition of $\mathbb{W}$. The bases for $\mathbb{V}$ and $\mathbb{W}$ to be used in the construction of the matrices in Table 3.1 can be taken as

$$\{\varphi_1 \ldots, \varphi_N\} = \left\{ M^{\boldsymbol{G}}_{\boldsymbol{n},\boldsymbol{p},\boldsymbol{i}} : \boldsymbol{i} \in \mathcal{I}_{\boldsymbol{n},\boldsymbol{p}} \right\}, \qquad N = N_{\boldsymbol{n},\boldsymbol{p}} = \#\mathcal{I}_{\boldsymbol{n},\boldsymbol{p}}, \tag{3.6}$$

$$\{\boldsymbol{\psi}_1, \ldots, \boldsymbol{\psi}_L\} = \left\{ (\underbrace{0, \ldots, 0}_{\alpha-1}, M^{\boldsymbol{G}}_{\boldsymbol{n},\boldsymbol{p},\boldsymbol{i}}, \underbrace{0, \ldots, 0}_{d-\alpha}) : \boldsymbol{i} \in \mathcal{I}^{\Gamma}_{\boldsymbol{n},\boldsymbol{p}},\ \alpha = 1, \ldots, d \right\}, \qquad L = d N^{\Gamma}_{\boldsymbol{n},\boldsymbol{p}} = d(\#\mathcal{I}^{\Gamma}_{\boldsymbol{n},\boldsymbol{p}}). \tag{3.7}$$

Remark 3.2. Standard immersed methods might suffer from ill-conditionings due to the boundary cut of the tensor-product mesh leading to tiny overlaps of some basis functions in the domain. This can be overcome by the use of so-called extended B-splines [20]. To improve the conditioning of the basis, the boundary B-splines with tiny overlap (i.e., less than one mesh element) are adjoined suitably to the surrounding B-splines with substantial overlap. The corresponding slightly smaller subspace meets all the usual requirements for standard approximations, and in particular it retains the optimal approximation order. In a nutshell, the extended B-splines are constructed as follows. We split the index set $\mathcal{I}_{\boldsymbol{n},\boldsymbol{p}} = \mathcal{I}^{i}_{\boldsymbol{n},\boldsymbol{p}} \cup \mathcal{I}^{b}_{\boldsymbol{n},\boldsymbol{p}}$, where $\mathcal{I}^{b}_{\boldsymbol{n},\boldsymbol{p}}$ contains the indices of the problematic boundary

B-splines with tiny overlap and $\mathcal{I}^i_{\boldsymbol{n},\boldsymbol{p}}$ contains all the other indices (called inner indices). For each $\boldsymbol{j} \in \mathcal{I}^b_{\boldsymbol{n},\boldsymbol{p}}$, we choose $\mathcal{I}^i(\boldsymbol{j}) = \{\boldsymbol{\ell}, \dots, \boldsymbol{\ell}+\boldsymbol{p}\} \subseteq \mathcal{I}^i_{\boldsymbol{n},\boldsymbol{p}}$ to be a subset of inner indices closest to $\boldsymbol{j}$ for some $\boldsymbol{\ell}$. Moreover, we set

$$e_{\boldsymbol{i},\boldsymbol{j}} = \prod_{\alpha=1}^{d} \prod_{\substack{\beta=0 \\ i_\alpha \neq \ell_\alpha+\beta}}^{p_\alpha} \frac{j_\alpha - \ell_\alpha - \beta}{i_\alpha - \ell_\alpha - \beta}, \qquad \boldsymbol{i} \in \mathcal{I}^i(\boldsymbol{j}).$$

These correspond to the values of the tensor-product Lagrange polynomials at $\boldsymbol{j}$ associated with $\mathcal{I}^i(\boldsymbol{j})$. Then, we define the extended B-splines as

$$M^{\boldsymbol{G},\mathrm{ext}}_{\boldsymbol{n},\boldsymbol{p},\boldsymbol{i}}(\boldsymbol{x}) = M^{\boldsymbol{G}}_{\boldsymbol{n},\boldsymbol{p},\boldsymbol{i}}(\boldsymbol{x}) + \sum_{\boldsymbol{j} \in \mathcal{J}^i(\boldsymbol{i})} e_{\boldsymbol{i},\boldsymbol{j}} M^{\boldsymbol{G}}_{\boldsymbol{n},\boldsymbol{p},\boldsymbol{j}}(\boldsymbol{x}), \qquad \boldsymbol{i} \in \mathcal{I}^i_{\boldsymbol{n},\boldsymbol{p}}, \tag{3.8}$$

where $\mathcal{J}^i(\boldsymbol{i}) = \{\boldsymbol{j} \in \mathcal{I}^b_{\boldsymbol{n},\boldsymbol{p}} : \boldsymbol{i} \in \mathcal{I}^i(\boldsymbol{j})\}$. For more details, we refer the reader to [19, 20].

4. Spectral analysis of immersed B-spline discretization matrices

In this section we describe the spectral symbol of the immersed discretization matrices based on mapped tensor-product B-spline basis functions and we study some of its properties. Afterwards, we exploit this spectral knowledge to design a specific CG preconditioner for the considered immersed discretization matrices. In what follows, we use the abbreviation SPD for symmetric positive definite and SPSD for symmetric positive semi-definite. If X, Y are two symmetric matrices of the same size, the notation $X > Y$ (resp., $X \geq Y$) means that $X - Y$ is SPD (resp., SPSD).

4.1. Definition of the spectral symbol

Let $\mathbb{Q}^d_+$ be the set of vectors in $\mathbb{Q}^d$ with positive components. Consider the matrices K^{uu}, K^{uu}_{in}, $K^{\sigma\sigma}$, $K^{u\sigma}$, $K^{\sigma u}$, $G^{u\sigma}$, $G^{\sigma u}$ resulting from the choice of the bases (3.6)–(3.7). It is understood that these matrices depend on the mesh fineness parameter $\boldsymbol{n}$, and hence each of them gives rise to a sequence of matrices for $\boldsymbol{n} = \boldsymbol{\nu} n = (\nu_1 n, \dots, \nu_d n)$, where $\boldsymbol{\nu} \in \mathbb{Q}^d_+$ and n varies in the infinite subset of $\mathbb{N}$ such that $\boldsymbol{n} = \boldsymbol{\nu} n \in \mathbb{N}^d$. It was shown in [10] that the corresponding sequences of matrices in (3.3) and (3.4), after suitable normalization, enjoy the same asymptotic spectral distribution as the sequence of matrices K^{uu}, and we recall the associated spectral symbol below. To this end, for every $\boldsymbol{p} \geq \boldsymbol{1}$, we define $H_{\boldsymbol{p}} : [-\pi, \pi]^d \to \mathbb{C}^{d \times d}$ by

$$H_{\boldsymbol{p}}(\boldsymbol{\theta}) = [H_{\boldsymbol{p},\alpha\beta}(\boldsymbol{\theta})]^d_{\alpha,\beta=1}, \tag{4.1}$$

$$H_{\boldsymbol{p},\alpha\beta}(\boldsymbol{\theta}) = \sum_{\boldsymbol{k} \in \mathbb{Z}^d} -\frac{\partial^2 M_{2\boldsymbol{p}+\boldsymbol{1}}}{\partial x_\alpha \partial x_\beta}(\boldsymbol{p} + \boldsymbol{1} + \boldsymbol{k})\, \mathrm{e}^{\mathrm{i}\boldsymbol{k}\cdot\boldsymbol{\theta}}, \qquad \alpha, \beta = 1, \dots, d. \tag{4.2}$$

Note that the series in (4.2) is actually a finite sum due to the compact support of $M_{2\boldsymbol{p}+\boldsymbol{1}}$. For a sufficiently regular geometry map $\boldsymbol{G}$, let

$$A_{\boldsymbol{G}} = (J_{\boldsymbol{G}})^{-1} A(\boldsymbol{G}) (J_{\boldsymbol{G}})^{-T},$$

where $J_{\boldsymbol{G}}$ is the Jacobian matrix of $\boldsymbol{G}$. Then, for every $\boldsymbol{p} \geq \boldsymbol{1}$ and $\boldsymbol{\nu} \in \mathbb{Q}^d_+$, we define $f^{\boldsymbol{\nu}}_{\boldsymbol{G},\boldsymbol{p}} : \boldsymbol{G}^{-1}(\Omega) \times [-\pi, \pi]^d \to \mathbb{C}$ by

$$f^{\boldsymbol{\nu}}_{\boldsymbol{G},\boldsymbol{p}}(\hat{\boldsymbol{x}}, \boldsymbol{\theta}) = \frac{\boldsymbol{\nu}(|\det(J_{\boldsymbol{G}}(\hat{\boldsymbol{x}}))| A_{\boldsymbol{G}}(\hat{\boldsymbol{x}}) \circ H_{\boldsymbol{p}}(\boldsymbol{\theta}))\boldsymbol{\nu}^T}{N(\boldsymbol{\nu})}, \tag{4.3}$$

where $\circ$ is the componentwise (Hadamard) product of matrices. The next theorem follows from [10, Theorem 4.1 and Remark 4.7].

Theorem 4.1. *Let $\boldsymbol{p} \geq \boldsymbol{1}$ and let $\boldsymbol{n} = \boldsymbol{\nu} n$, where $\boldsymbol{\nu} \in \mathbb{Q}^d_+$ and n varies in the infinite subset of $\mathbb{N}$ such that $\boldsymbol{n} = \boldsymbol{\nu} n \in \mathbb{N}^d$. Suppose that $\boldsymbol{G}$ is a sufficiently regular geometry map and suppose that the matrix $A = [a_{\alpha\beta}]^d_{\alpha,\beta=1}$ is symmetric and each component $a_{\alpha\beta}$ belongs to $L^1(\Omega)$. Then, for the matrix K^{uu} and the matrices in* (3.3) *and* (3.4) *resulting from the choice of the bases* (3.6)–(3.7) *we have*

$$\{n^{d-2} K^{uu}\}_n \sim_{\sigma,\lambda} f^{\boldsymbol{\nu}}_{\boldsymbol{G},\boldsymbol{p}}, \tag{4.4}$$

$$\left\{ n^{d-2} \begin{bmatrix} K^{uu} + K^{uu}_{\mathrm{in}} & K^{u\sigma} + G^{u\sigma} \\ K^{\sigma u} + G^{\sigma u} & K^{\sigma\sigma} \end{bmatrix} \right\}_n \sim_{\sigma,\lambda} f^{\boldsymbol{\nu}}_{\boldsymbol{G},\boldsymbol{p}}, \tag{4.5}$$

$$\{n^{d-2}[K^{uu} + K^{uu}_{\mathrm{in}} - (K^{u\sigma} + G^{u\sigma})(K^{\sigma\sigma})^{-1}(K^{\sigma u} + G^{\sigma u})]\}_n \sim_{\sigma,\lambda} f^{\boldsymbol{\nu}}_{\boldsymbol{G},\boldsymbol{p}}, \tag{4.6}$$

where $f^{\boldsymbol{\nu}}_{\boldsymbol{G},\boldsymbol{p}}$ is defined in (4.3).

Remark 4.1. The symbol in (4.3) is essentially the same as the symbol in the untrimmed case when a suitable natural restriction of the parametric domain is considered; see, e.g., [11, 12]. Moreover, as explained in [10, Remark 4.3] and [11, Section 4.6], there is a structural connection between the expression of the symbol and the expression of the differential operator.

Remark 4.2. It was pointed out in [10, Remark 4.6] that the result in Theorem 4.1 remains valid when considering the extended B-splines (3.8) instead of the standard B-splines (3.5).

4.2. Properties of the spectral symbol

In order to study the properties of the spectral symbol $f^{\boldsymbol{\nu}}_{\boldsymbol{G},\boldsymbol{p}}$ in (4.3), let us first recall from [10, Remark 4.4] that the matrix $H_{\boldsymbol{p}}(\boldsymbol{\theta}) = [H_{\boldsymbol{p},\alpha\beta}(\boldsymbol{\theta})]_{\alpha,\beta=1}^{d}$ in (4.1)–(4.2) can be written as

$$H_{\boldsymbol{p},\alpha\beta}(\boldsymbol{\theta}) = \begin{cases} f_{p_\alpha}(\theta_\alpha) \displaystyle\prod_{\substack{r=1 \\ r\neq\alpha}}^{d} h_{p_r}(\theta_r), & \text{if } \alpha = \beta, \\ g_{p_\alpha}(\theta_\alpha) g_{p_\beta}(\theta_\beta) \displaystyle\prod_{\substack{r=1 \\ r\neq\alpha,\beta}}^{d} h_{p_r}(\theta_r), & \text{if } \alpha \neq \beta, \end{cases}$$

where the functions $h_p, g_p, f_p : [-\pi,\pi] \to \mathbb{R}$ are given by

$$h_p(\theta) = \sum_{k\in\mathbb{Z}} M_{2p+1}(p+1+k)\mathrm{e}^{\mathrm{i}k\theta} = M_{2p+1}(p+1) + 2\sum_{k=1}^{p} M_{2p+1}(p+1-k)\cos(k\theta), \qquad p \geq 0, \tag{4.7}$$

$$g_p(\theta) = \sum_{k\in\mathbb{Z}} M'_{2p+1}(p+1+k)\mathrm{e}^{\mathrm{i}k\theta} = -2\sum_{k=1}^{p} M'_{2p+1}(p+1-k)\sin(k\theta), \qquad p \geq 1, \tag{4.8}$$

$$f_p(\theta) = \sum_{k\in\mathbb{Z}} M''_{2p+1}(p+1+k)\mathrm{e}^{\mathrm{i}k\theta} = -M''_{2p+1}(p+1) - 2\sum_{k=1}^{p} M''_{2p+1}(p+1-k)\cos(k\theta), \qquad p \geq 1. \tag{4.9}$$

We remark that $H_{\boldsymbol{p}}$ coincides with the matrix defined in [11, Eq. (4.1)] and h_p, g_p, f_p coincide with the functions defined in [11, Eqs. (4.2)–(4.4)]. The properties of $H_{\boldsymbol{p}}$ and h_p, g_p, f_p were investigated in [7, 8, 9, 11, 12]. More specifically, the main results were obtained in [7, Section 3], [8, Theorem 3.4 and Lemma A.2], [9, Lemmas 6–7], and [12, Theorem 2.2]; we collect them in Theorems 4.2 and 4.3 for the reader's convenience.

Theorem 4.2. *For every $d \geq 1$ and every $\boldsymbol{p} \geq \mathbf{1}$, the $d \times d$ matrix $H_{\boldsymbol{p}}(\boldsymbol{\theta})$ defined in* (4.1)–(4.2) *is SPSD for all $\boldsymbol{\theta} \in [-\pi,\pi]^d$ and it is SPD for all $\boldsymbol{\theta} \in [-\pi,\pi]^d$ with $\prod_{i=1}^{d} \theta_i \neq 0$.*

To simplify the statement of Theorem 4.3, for every $p \geq 0$ we define the functions $L_p, U_p : [-\pi,\pi] \to \mathbb{R}$ as follows:

$$L_p(\theta) = \left(\frac{2-2\cos\theta}{\theta^2}\right)^{p+1}, \tag{4.10}$$

$$U_p(\theta) = \left(\frac{2-2\cos\theta}{\theta^2}\right)^{p+1} + \left(\frac{\pi^2}{48} - 1\right)\left(\frac{2-2\cos\theta}{\pi^2}\right)^{p+1}. \tag{4.11}$$

Note that the function L_p is even and strictly decreasing on $[0,\pi]$ with $L_p(0) = 1$ and $L_p(\pi) = 4/\pi^2$.

Theorem 4.3. *For every $p \geq 0$, let $L_p, U_p : [-\pi,\pi] \to \mathbb{R}$ be defined as in* (4.10)–(4.11).

1. *For every $p \geq 0$, the function $h_p : [-\pi,\pi] \to \mathbb{R}$ in* (4.7) *satisfies the following properties.*
   - *For every $\theta \in [-\pi,\pi]$,*
   $$h_p(\theta) = (2-2\cos\theta)^{p+1} \sum_{k\in\mathbb{Z}} \frac{1}{(\theta+2k\pi)^{2p+2}}.$$

- $L_p(\theta) \le h_p(\theta) \le \min(1, U_p(\theta))$ *for every* $\theta \in [-\pi, \pi]$.
- h_p *is even and strictly decreasing on* $[0, \pi]$ *with* $\max_{\theta\in[-\pi,\pi]} h_p(\theta) = h_p(0) = 1$ *and*

$$\left(\frac{4}{\pi^2}\right)^{p+1} \le \min_{\theta\in[-\pi,\pi]} h_p(\theta) = h_p(\pi) \le \frac{1}{2^p} = \frac{h_p(\pi)}{h_p(\pi/2)}.$$

2. *For every* $p \ge 1$, *the function* $g_p : [-\pi, \pi] \to \mathbb{R}$ *in* (4.8) *satisfies the following properties.*
   - *For every* $\theta \in [-\pi, \pi]$,
   $$g_p(\theta) = -(2 - 2\cos\theta)^{p+1} \sum_{k\in\mathbb{Z}} \frac{1}{(\theta + 2k\pi)^{2p+1}}.$$
   - *For every* $\theta \in [-\pi, \pi]$,
   $$\frac{(2 - 2\cos\theta)^{p+1}}{|\theta|^{2p+1}} - \frac{(2 - 2\cos\theta)^{p+1}}{\pi^{2p+1}} \le |g_p(\theta)| \le \frac{(2 - 2\cos\theta)^{p+1}}{|\theta|^{2p+1}}.$$
   - g_p *is odd and its zeros are given by* $g_p(-\pi) = g_p(0) = g_p(\pi) = 0$.
3. *For every* $p \ge 1$, *the function* $f_p : [-\pi, \pi] \to \mathbb{R}$ *in* (4.9) *satisfies the following properties.*
   - *For every* $\theta \in [-\pi, \pi]$,
   $$f_p(\theta) = (2 - 2\cos\theta)^{p+1} \sum_{k\in\mathbb{Z}} \frac{1}{(\theta + 2k\pi)^{2p}} = (2 - 2\cos\theta) h_{p-1}(\theta).$$
   - $(2 - 2\cos\theta) L_{p-1}(\theta) \le f_p(\theta) \le (2 - 2\cos\theta)\min(1, U_{p-1}(\theta))$ *for every* $\theta \in [-\pi, \pi]$.
   - f_p *is even with*
   $$\max_{\theta\in[-\pi,\pi]} f(\theta) = M_{f_p} \le \min\left(4, \frac{8}{p+1} + \left(\frac{\pi^4}{12} - 4\right)\left(\frac{4}{\pi^2}\right)^p\right)$$
   and $\min_{\theta\in[-\pi,\pi]} f(\theta) = f(0) = 0$. *Moreover,* $\theta = 0$ *is the unique zero of* f_p *over* $[-\pi, \pi]$ *and*
   $$\frac{f_p(\pi)}{M_{f_p}} \le \frac{f_p(\pi)}{f_p(\pi/2)} = \frac{4}{2^p}.$$

We are now ready to address the symbol $f^{\boldsymbol{\nu}}_{\boldsymbol{G},\boldsymbol{p}}$ in (4.3) and derive a result that is a generalization of [11, Theorem 5.4] to the case where the parametric domain $[0, 1]^d$ is replaced by $\boldsymbol{G}^{-1}(\Omega)$. Note that the variables $(\hat{\boldsymbol{x}}, \boldsymbol{\theta})$ in (4.3) vary in $\boldsymbol{G}^{-1}(\Omega) \times [-\pi, \pi]^d$ for the given open Lipschitz domain $\Omega \subset \mathbb{R}^d$ and not in $[0, 1]^d \times [-\pi, \pi]^d$ as in [11, Theorem 5.4]. In view of what follows, we observe that $f^{\boldsymbol{\nu}}_{\boldsymbol{G},\boldsymbol{p}}$ is independent of the $\hat{\boldsymbol{x}}$ variables in the case where $\Omega = (0, 1)^d$, $\boldsymbol{G}$ is the identity map, and $A = I_d$ is the identity matrix. It is natural to consider its restriction to the domain $[-\pi, \pi]^d$, i.e., the function $f^{\boldsymbol{\nu}}_{\boldsymbol{p}} : [-\pi, \pi]^d \to \mathbb{R}$,

$$f^{\boldsymbol{\nu}}_{\boldsymbol{p}}(\boldsymbol{\theta}) = \frac{\boldsymbol{\nu}(I_d \circ H_{\boldsymbol{p}}(\boldsymbol{\theta}))\boldsymbol{\nu}^T}{N(\boldsymbol{\nu})} = \frac{1}{N(\boldsymbol{\nu})} \sum_{\alpha=1}^{d} \nu_\alpha^2 f_{p_\alpha}(\theta_\alpha) \prod_{\substack{r=1 \\ r\ne\alpha}}^{d} h_{p_r}(\theta_r). \tag{4.12}$$

By Theorem 4.3, we have

$$c_{\boldsymbol{p},\boldsymbol{\nu}} \sum_{\alpha=1}^{d} (2 - 2\cos\theta_\alpha) \le f^{\boldsymbol{\nu}}_{\boldsymbol{p}}(\boldsymbol{\theta}) \le C_{\boldsymbol{p},\boldsymbol{\nu}} \sum_{\alpha=1}^{d} (2 - 2\cos\theta_\alpha), \tag{4.13}$$

where

$$c_{\boldsymbol{p},\boldsymbol{\nu}} = \left(\frac{4}{\pi^2}\right)^{p_1+\ldots+p_d+d-1} \frac{\min(\boldsymbol{\nu}^2)}{N(\boldsymbol{\nu})}, \qquad C_{\boldsymbol{p},\boldsymbol{\nu}} = \frac{\max(\boldsymbol{\nu}^2)}{N(\boldsymbol{\nu})}.$$

Since the ratio $C_{\boldsymbol{p},\boldsymbol{\nu}}/c_{\boldsymbol{p},\boldsymbol{\nu}}$ increases with $\max(\boldsymbol{\nu})/\min(\boldsymbol{\nu})$, the best relative bounds in (4.13) with respect to $\boldsymbol{\nu}$ are obtained when all entries of $\boldsymbol{\nu}$ are equal, i.e., when the scaled tensor-product mesh $\frac{1}{\boldsymbol{n}}\Delta_d$ is formed by squares.

Theorem 4.4. *Let $\boldsymbol{p}, \boldsymbol{\nu}, \boldsymbol{G}, A$ be defined as in Theorem 4.1. Then, the spectral symbol $f^{\boldsymbol{\nu}}_{\boldsymbol{G},\boldsymbol{p}} : \boldsymbol{G}^{-1}(\Omega)\times[-\pi,\pi]^d \to \mathbb{R}$ in (4.3) satisfies the following properties.*

1. For every $(\hat{\boldsymbol{x}}, \boldsymbol{\theta}) \in \boldsymbol{G}^{-1}(\Omega) \times [-\pi,\pi]^d$, we have

$$\begin{aligned} f^{\boldsymbol{\nu}}_{\boldsymbol{G},\boldsymbol{p}}(\hat{\boldsymbol{x}}, \boldsymbol{\theta}) &\geq \lambda_{\min}(A_{\boldsymbol{G}}(\hat{\boldsymbol{x}}))|\det(J_{\boldsymbol{G}}(\hat{\boldsymbol{x}}))| f^{\boldsymbol{\nu}}_{\boldsymbol{p}}(\boldsymbol{\theta}), \\ f^{\boldsymbol{\nu}}_{\boldsymbol{G},\boldsymbol{p}}(\hat{\boldsymbol{x}}, \boldsymbol{\theta}) &\leq \lambda_{\max}(A_{\boldsymbol{G}}(\hat{\boldsymbol{x}}))|\det(J_{\boldsymbol{G}}(\hat{\boldsymbol{x}}))| f^{\boldsymbol{\nu}}_{\boldsymbol{p}}(\boldsymbol{\theta}). \end{aligned} \tag{4.14}$$

As a consequence, if

$$cI_d \leq A_{\boldsymbol{G}}(\hat{\boldsymbol{x}})|\det(J_{\boldsymbol{G}}(\hat{\boldsymbol{x}}))| \leq CI_d \tag{4.15}$$

for every $\hat{\boldsymbol{x}} \in \boldsymbol{G}^{-1}(\Omega)$ and some positive constants c and C, then

$$c f^{\boldsymbol{\nu}}_{\boldsymbol{p}}(\boldsymbol{\theta}) \leq f^{\boldsymbol{\nu}}_{\boldsymbol{G},\boldsymbol{p}}(\hat{\boldsymbol{x}}, \boldsymbol{\theta}) \leq C f^{\boldsymbol{\nu}}_{\boldsymbol{p}}(\boldsymbol{\theta})$$

for every $(\hat{\boldsymbol{x}}, \boldsymbol{\theta}) \in \boldsymbol{G}^{-1}(\Omega) \times [-\pi,\pi]^d$.

2. If A is SPSD on Ω, then $f^{\boldsymbol{\nu}}_{\boldsymbol{G},\boldsymbol{p}}$ is non-negative on $\boldsymbol{G}^{-1}(\Omega) \times [-\pi,\pi]^d$.

Proof. 1. It is clear that

$$\lambda_{\min}(A_{\boldsymbol{G}}(\hat{\boldsymbol{x}}))I_d \leq A_{\boldsymbol{G}}(\hat{\boldsymbol{x}}) \leq \lambda_{\max}(A_{\boldsymbol{G}}(\hat{\boldsymbol{x}}))I_d$$

for all $\hat{\boldsymbol{x}} \in \boldsymbol{G}^{-1}(\Omega)$. In particular, the matrices $A_{\boldsymbol{G}}(\hat{\boldsymbol{x}}) - \lambda_{\min}(A_{\boldsymbol{G}}(\hat{\boldsymbol{x}}))I_d$ and $\lambda_{\max}(A_{\boldsymbol{G}}(\hat{\boldsymbol{x}}))I_d - A_{\boldsymbol{G}}(\hat{\boldsymbol{x}})$ are SPSD for all $\hat{\boldsymbol{x}} \in \boldsymbol{G}^{-1}(\Omega)$. Moreover, we know from Theorem 4.2 that $H_{\boldsymbol{p}}(\boldsymbol{\theta})$ is SPSD for all $\boldsymbol{\theta} \in [-\pi,\pi]^d$. Thus, for all $(\hat{\boldsymbol{x}}, \boldsymbol{\theta}) \in \boldsymbol{G}^{-1}(\Omega) \times [-\pi,\pi]^d$,

$$f^{\boldsymbol{\nu}}_{\boldsymbol{G},\boldsymbol{p}}(\hat{\boldsymbol{x}}, \boldsymbol{\theta}) - \lambda_{\min}(J_{\boldsymbol{G}}(\hat{\boldsymbol{x}}))|\det(J_{\boldsymbol{G}}(\hat{\boldsymbol{x}}))| f^{\boldsymbol{\nu}}_{\boldsymbol{p}}(\boldsymbol{\theta}) = \frac{\boldsymbol{\nu}(|\det(J_{\boldsymbol{G}}(\hat{\boldsymbol{x}}))|(A_{\boldsymbol{G}}(\hat{\boldsymbol{x}}) - \lambda_{\min}(A_{\boldsymbol{G}}(\hat{\boldsymbol{x}}))I_d) \circ H_{\boldsymbol{p}}(\boldsymbol{\theta}))\boldsymbol{\nu}^T}{N(\boldsymbol{\nu})} \geq 0,$$

where the last inequality follows from the fact that $X \circ Y$ is SPSD whenever X and Y are SPSD, because $X \circ Y$ is a principal submatrix of the Kronecker tensor product $X \otimes Y$, which is SPSD whenever X and Y are SPSD; see, e.g., [18, Example 2.13].

2. Suppose that A is SPSD on Ω. Then, $A_{\boldsymbol{G}} = (J_{\boldsymbol{G}})^{-1}A(\boldsymbol{G})(J_{\boldsymbol{G}})^{-T}$ is SPSD on $\boldsymbol{G}^{-1}(\Omega)$. In particular, we have $\lambda_{\min}(A_{\boldsymbol{G}}(\hat{\boldsymbol{x}})) \geq 0$ for all $\hat{\boldsymbol{x}} \in \boldsymbol{G}^{-1}(\Omega)$. Since $f^{\boldsymbol{\nu}}_{\boldsymbol{p}}(\boldsymbol{\theta}) \geq 0$ for all $\boldsymbol{\theta} \in [-\pi,\pi]^d$ by (4.13), we infer from (4.14) that $f^{\boldsymbol{\nu}}_{\boldsymbol{G},\boldsymbol{p}} \geq 0$ on $\boldsymbol{G}^{-1}(\Omega) \times [-\pi,\pi]^d$. □

Remark 4.3. Two positive constants c and C satisfying (4.15) exist if and only if

$$c_* = \inf_{\hat{\boldsymbol{x}} \in \boldsymbol{G}^{-1}(\Omega)} \lambda_{\min}(A_{\boldsymbol{G}}(\hat{\boldsymbol{x}}))|\det(J_{\boldsymbol{G}}(\hat{\boldsymbol{x}}))| > 0, \qquad C_* = \sup_{\hat{\boldsymbol{x}} \in \boldsymbol{G}^{-1}(\Omega)} \lambda_{\max}(A_{\boldsymbol{G}}(\hat{\boldsymbol{x}}))|\det(J_{\boldsymbol{G}}(\hat{\boldsymbol{x}}))| < \infty. \tag{4.16}$$

In this case, c_* and C_* are also the best constants for which (4.15) holds. Note that, for the conditions (4.16) to be satisfied, it is necessary that the map $\boldsymbol{G}$ is sufficiently regular. In particular, there must be no singularity points $\hat{\boldsymbol{x}} \in \boldsymbol{G}^{-1}(\Omega)$ such that $\det(J_{\boldsymbol{G}}(\hat{\boldsymbol{x}})) = 0$.

4.3. Preconditioning of immersed B-spline discretization matrices

Here we illustrate how Theorems 4.1 and 4.4 could be used to identify potentially fast preconditioners for the linear system (3.4), i.e., for the matrix

$$K^{uu} + K^{uu}_{\text{in}} - (K^{u\sigma} + G^{u\sigma})(K^{\sigma\sigma})^{-1}(K^{\sigma u} + G^{\sigma u}). \tag{4.17}$$

Suppose that the assumptions of Theorem 4.1 are satisfied. From (4.4) and (4.6) we know that the asymptotic spectral distributions of the sequence of matrices $n^{d-2}K^{uu}$ and the sequence of matrices (4.17) multiplied by n^{d-2} can be described by the same symbol $f^{\boldsymbol{\nu}}_{\boldsymbol{G},\boldsymbol{p}}$. This suggests that K^{uu} might be suited as a candidate preconditioner for (4.17). However, this (naive) choice can be ruled out in practice because it can be verified that K^{uu} is a singular matrix.

To identify a potentially fast and non-singular preconditioner, we proceed as follows. Suppose that the assumptions of Theorem 4.1 are satisfied and

$$cI_d \leq A_{\boldsymbol{G}}(\hat{\boldsymbol{x}})|\det(J_{\boldsymbol{G}}(\hat{\boldsymbol{x}}))| \leq CI_d$$

for every $\hat{\boldsymbol{x}} \in \boldsymbol{G}^{-1}(\Omega)$ and some constants $c, C > 0$ (see also Remark 4.3). We recall from [10, Remark 4.7] that K^{uu} is explicitly given by

$$K^{uu} = \left[\int_{\boldsymbol{G}^{-1}(\Omega)} A_{\boldsymbol{G}} \, \nabla M_{\boldsymbol{n},\boldsymbol{p},\boldsymbol{j}} \cdot \nabla M_{\boldsymbol{n},\boldsymbol{p},\boldsymbol{i}} \, |\det(J_{\boldsymbol{G}})| \right]_{\boldsymbol{i},\boldsymbol{j} \in \mathcal{I}_{\boldsymbol{n},\boldsymbol{p}}}.$$

Let

$$\widetilde{K}^{uu} = \left[\int_{\mathbb{R}^d} \nabla M_{\boldsymbol{n},\boldsymbol{p},\boldsymbol{j}} \cdot \nabla M_{\boldsymbol{n},\boldsymbol{p},\boldsymbol{i}} \right]_{\boldsymbol{i},\boldsymbol{j} \in \mathcal{I}_{\boldsymbol{n},\boldsymbol{p}}}. \tag{4.18}$$

Using arguments from the theory of reduced GLT sequences as in the proof of (4.4), it can be shown that

$$\{n^{d-2} \widetilde{K}^{uu}\}_n \sim_{\sigma,\lambda} f^{\boldsymbol{\nu}}_{\boldsymbol{p}}.$$

Moreover, the matrix $\widetilde{K}^{uu}$ is non-singular. Indeed, this can be seen by the fact that $n^{d-2}\widetilde{K}^{uu}$ is a principal submatrix of a so-called d-level Toeplitz matrix T generated by the symbol $f^{\boldsymbol{\nu}}_{\boldsymbol{p}}$. Since $f^{\boldsymbol{\nu}}_{\boldsymbol{p}}$ is non-negative by (4.13), the theory of multilevel Toeplitz matrices [15, Chapter 3] and Cauchy's interlacing theorem [4, Corollary III.1.5] imply that both T and $n^{d-2}\widetilde{K}^{uu}$ are SPD, with the minimum (resp., maximum) eigenvalue of $n^{d-2}\widetilde{K}^{uu}$ larger (resp., smaller) than the minimum (resp., maximum) eigenvalue of T.

By Theorem 4.4 and (4.13), we have

$$c \leq (f^{\boldsymbol{\nu}}_{\boldsymbol{p}}(\boldsymbol{\theta}))^{-1} f^{\boldsymbol{\nu}}_{\boldsymbol{G},\boldsymbol{p}}(\hat{\boldsymbol{x}}, \boldsymbol{\theta}) \leq C \tag{4.19}$$

for every $(\hat{\boldsymbol{x}}, \boldsymbol{\theta}) \in \boldsymbol{G}^{-1}(\Omega) \times [-\pi, \pi]^d$ with $\boldsymbol{\theta} \neq \boldsymbol{0}$. Therefore, again relying on the theory of reduced GLT sequences, we expect that the sequence of preconditioned matrices

$$(\widetilde{K}^{uu})^{-1} \left[K^{uu} + K^{uu}_{\text{in}} - (K^{u\sigma} + G^{u\sigma})(K^{\sigma\sigma})^{-1}(K^{\sigma u} + G^{\sigma u}) \right] \tag{4.20}$$

has an asymptotic spectral distribution described by the preconditioned symbol $(f^{\boldsymbol{\nu}}_{\boldsymbol{p}})^{-1} f^{\boldsymbol{\nu}}_{\boldsymbol{G},\boldsymbol{p}}$, whose essential range is contained in the interval $[c, C]$ by (4.19). This implies that the eigenvalues of the sequence of matrices (4.20) are weakly clustered at $[c, C]$; see [14, Theorem 3.1]. Consequently, in view of the convergence properties of the CG and GMRES methods [3, Section 2.2], we may predict that the preconditioned CG (PCG) and preconditioned GMRES (PGMRES) methods with preconditioner $\widetilde{K}^{uu}$ for solving a linear system with coefficient matrix (4.17) have a good convergence rate and the number of iterations for reaching a preassigned accuracy ε is independent of (or only weakly dependent on) the matrix size.

Remark 4.4. When considering the extended B-splines (3.8) instead of the standard B-splines (3.5), the proposed preconditioner $\widetilde{K}^{uu}$ is still given by (4.18), with the only difference that $\boldsymbol{i}$ and $\boldsymbol{j}$ do not vary in the set $\mathcal{I}_{\boldsymbol{n},\boldsymbol{p}}$ but in the set $\mathcal{I}^i_{\boldsymbol{n},\boldsymbol{p}}$ defined in Remark 3.2.

5. Numerical experiments

In this section we numerically illustrate the spectral distribution result in (4.6) by comparing the spectrum of the matrix in the left-hand side with uniform samples of the spectral symbol $f^{\boldsymbol{\nu}}_{\boldsymbol{G},\boldsymbol{p}}$; see Remark 2.1. Moreover, we check the validity of the lower and upper bounds for the spectral symbol $f^{\boldsymbol{\nu}}_{\boldsymbol{G},\boldsymbol{p}}$ given in (4.14). Finally, we compare the number of CG and PCG iterations for solving the linear system (3.4) up to a precision of 10^{-6}, where the preconditioner for the PCG method is the matrix $\widetilde{K}^{uu}$ defined in (4.18).

In all the examples, we take $d = 2$, $\boldsymbol{p} = (p, p)$, $\boldsymbol{n} = (n, n)$ and $\eta = 2$. In this case, (4.6) reads

$$\{K^{uu} + K^{uu}_{\text{in}} - (K^{u\sigma} + G^{u\sigma})(K^{\sigma\sigma})^{-1}(K^{\sigma u} + G^{\sigma u})\}_n \sim_{\sigma,\lambda} \mathbf{1}(|\det(J_{\boldsymbol{G}}(\hat{x}_1, \hat{x}_2))| A_{\boldsymbol{G}}(\hat{x}_1, \hat{x}_2) \circ H_{(p,p)}(\theta_1, \theta_2))\mathbf{1}^T, \tag{5.1}$$

with

$$H_{(p,p)}(\theta_1, \theta_2) = \begin{bmatrix} f_p(\theta_1)h_p(\theta_2) & g_p(\theta_1)g_p(\theta_2) \\ g_p(\theta_1)g_p(\theta_2) & h_p(\theta_1)f_p(\theta_2) \end{bmatrix},$$

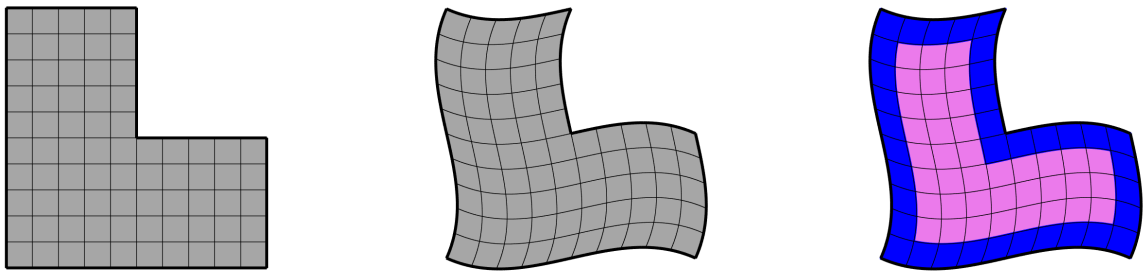

(a) $\hat{\Omega}$ (grey) (b) Ω (grey) (c) Ω_{in} (magenta) and $\Omega_{\Gamma,\text{in}}$ (blue)

Figure 5.1: Example 5.1: The parametric domain $\hat{\Omega}$, the physical domain Ω, and a possible mesh.

and h_p, g_p, f_p defined as in (4.7)–(4.9); and the bounds in (4.14) read

$$\begin{aligned}
&\mathbf{1}(|\det(J_{\boldsymbol{G}}(\hat{x}_1,\hat{x}_2))|A_{\boldsymbol{G}}(\hat{x}_1,\hat{x}_2)\circ H_{(p,p)}(\theta_1,\theta_2))\mathbf{1}^T\\
&\qquad \geq \lambda_{\min}(A_{\boldsymbol{G}}(\hat{x}_1,\hat{x}_2))|\det(J_{\boldsymbol{G}}(\hat{x}_1,\hat{x}_2))|(f_p(\theta_1)h_p(\theta_2)+h_p(\theta_1)f_p(\theta_2)),\\
&\mathbf{1}(|\det(J_{\boldsymbol{G}}(\hat{x}_1,\hat{x}_2))|A_{\boldsymbol{G}}(\hat{x}_1,\hat{x}_2)\circ H_{(p,p)}(\theta_1,\theta_2))\mathbf{1}^T\\
&\qquad \leq \lambda_{\max}(A_{\boldsymbol{G}}(\hat{x}_1,\hat{x}_2))|\det(J_{\boldsymbol{G}}(\hat{x}_1,\hat{x}_2))|(f_p(\theta_1)h_p(\theta_2)+h_p(\theta_1)f_p(\theta_2)),
\end{aligned} \tag{5.2}$$

for every $(\hat{x}_1,\hat{x}_2,\theta_1,\theta_2)\in \boldsymbol{G}^{-1}(\Omega)\times[-\pi,\pi]^2$. The values of p and n, the parametric domain $\hat{\Omega}$, the geometry map $\boldsymbol{G}:\hat{\Omega}\to\overline{\Omega}$, the matrix of diffusion coefficients A, and the data f and g in (3.1) to construct the linear system (3.4) are specified in each example. The definition of the physical domain Ω follows immediately from $\hat{\Omega}$ and $\boldsymbol{G}$. We only focus on the use of the extended B-spline basis (see Remarks 3.2, 4.2, and 4.4), because it is preferred over the standard B-spline basis for immersed methods in a practical context [20, 23]. The corresponding matrix in the left-hand side of (5.1) will be denoted by $L_{n,p}^{\boldsymbol{G},\text{ext}}$. For convenience of computation, we replace the symbol in (5.1) with its monotone rearrangement on the interval $[0,1]$; see [16, Remark A.1]. When comparing with the eigenvalues, we assume that the latter are sorted in non-decreasing order and positioned at $\frac{i}{s}$, $i=1,\dots,s$, where $s=N_{(n,n),(p,p)}$ is the matrix size.

Example 5.1. Let $\hat{\Omega}$ be the L-shaped domain with vertices $(0,1)$, $(0,0)$, $(1,0)$, $(1,\frac{1}{2})$, $(\frac{1}{2},\frac{1}{2})$, $(\frac{1}{2},1)$, and

$$\begin{aligned}
\boldsymbol{G}(\hat{x}_1,\hat{x}_2) &= \begin{bmatrix}\hat{x}_1-\frac{9}{20}\hat{x}_2(\hat{x}_2-1)(2\hat{x}_2-1)\\ \hat{x}_2-\frac{9}{20}\hat{x}_1(\hat{x}_1-1)(2\hat{x}_1-1)\end{bmatrix}, \quad (\hat{x}_1,\hat{x}_2)\in\hat{\Omega},\\
A(x_1,x_2) &= I_2=\begin{bmatrix}1&0\\0&1\end{bmatrix}, \quad (x_1,x_2)\in\Omega,\\
\mathrm{f}(x_1,x_2) &= 5\cos(x_1+2x_2), \quad (x_1,x_2)\in\Omega,\\
\mathrm{g}(x_1,x_2) &= \cos(x_1+2x_2), \quad (x_1,x_2)\in\Gamma=\partial\Omega.
\end{aligned}$$

The domains $\hat{\Omega}$ and Ω are illustrated in Figure 5.1. Note that in this case the extended B-splines defined in (3.8) are actually all standard (mapped) cardinal B-splines as defined in (3.5) for even n. The comparison between the eigenvalues of the matrix $L_{n,p}^{\boldsymbol{G},\text{ext}}$ and the monotone rearrangement of the symbol $\mathbf{1}(|\det(J_{\boldsymbol{G}}(\hat{x}_1,\hat{x}_2))|A_{\boldsymbol{G}}(\hat{x}_1,\hat{x}_2)\circ H_{(p,p)}(\theta_1,\theta_2))\mathbf{1}^T$ is shown in Figure 5.2 for different values of p and even n. Some large eigenvalues (outliers) have been cut from the figures in order to allow for a better visualization of the matching between the other eigenvalues and the monotone rearrangement of the symbol. The comparison between the number of CG and PCG iterations for solving the linear system (3.4) up to a precision of 10^{-6} is shown in Table 5.1 for $p=1,2$ and different even values of n. We see that the number of PCG iterations is considerably lower than the number of CG iterations for $p=1,2$ and large n. For $p>2$, we numerically checked that the number of PCG iterations remains averagely lower than the number of CG iterations, but the difference is not as significant as in the case $p=1,2$, showing that the preconditioner $\widetilde{K}^{uu}$ is more effective for low degrees than for high degrees.

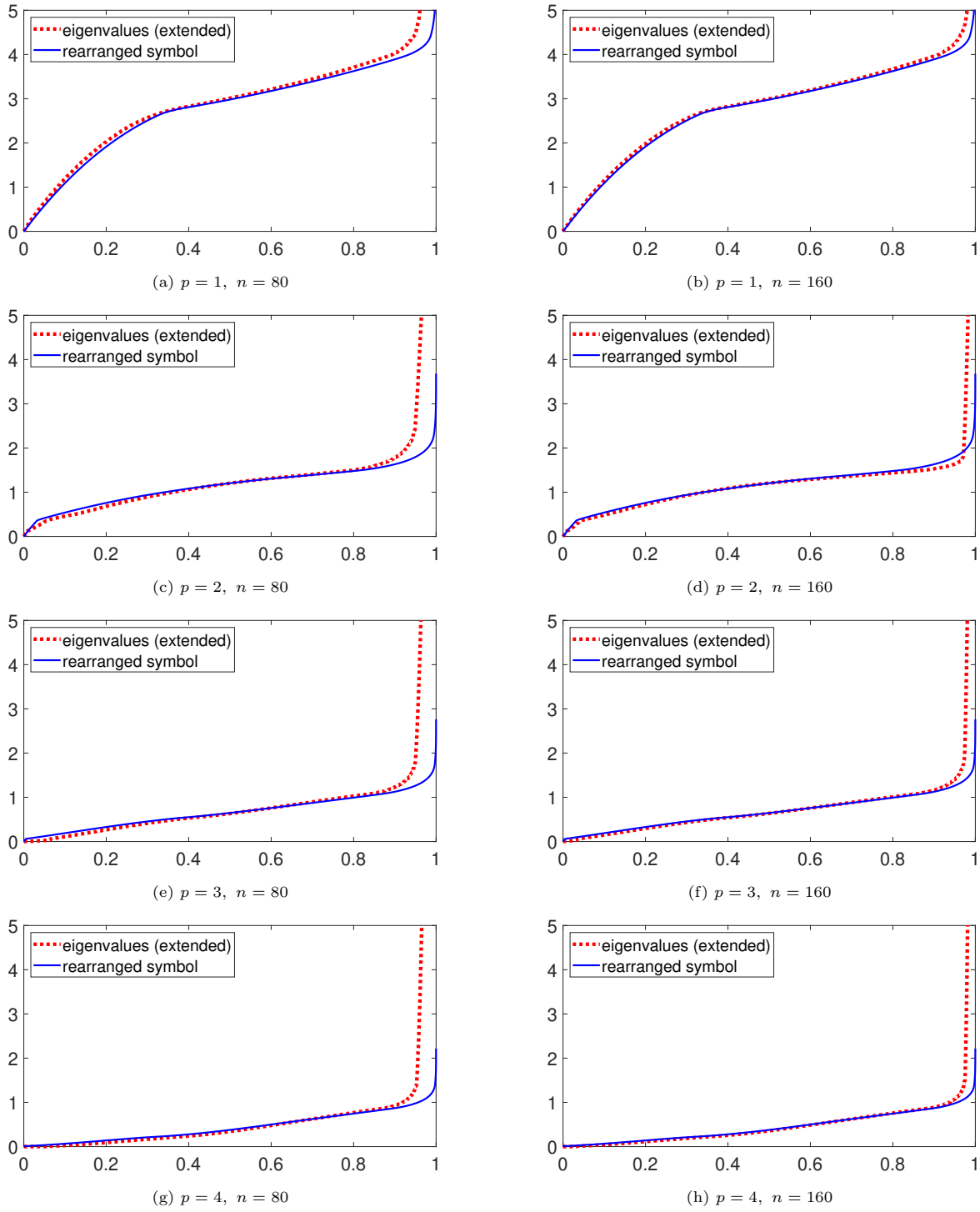

(a) $p = 1,\ n = 80$ (b) $p = 1,\ n = 160$

(c) $p = 2,\ n = 80$ (d) $p = 2,\ n = 160$

(e) $p = 3,\ n = 80$ (f) $p = 3,\ n = 160$

(g) $p = 4,\ n = 80$ (h) $p = 4,\ n = 160$

Figure 5.2: Example 5.1: Comparison between the eigenvalues of the matrix $L_{n,p}^{\boldsymbol{G},\text{ext}}$ (extended B-spline basis) and the monotone rearrangement of the symbol $\mathbf{1}(|\det(J_{\boldsymbol{G}}(\hat{x}_1,\hat{x}_2))|A_{\boldsymbol{G}}(\hat{x}_1,\hat{x}_2)\circ H_{(p,p)}(\theta_1,\theta_2))\mathbf{1}^T$ for $p = 1,2,3,4$ and $n = 80, 160$.

Table 5.1: Example 5.1: Number of CG and PCG iterations for solving the linear system (3.4) in the case of the extended B-spline basis up to a precision of 10^{-6} for $p = 1, 2$ and $n = 20, 40, 80, 160$.

(a) $p = 1$

n	CG iterations	PCG iterations
20	43	22
40	84	23
80	164	23
160	323	23

(b) $p = 2$

n	CG iterations	PCG iterations
20	84	83
40	95	97
80	183	105
160	360	109

Table 5.2: Example 5.2: Number of CG and PCG iterations for solving the linear system (3.4) in the case of the extended B-spline basis up to a precision of 10^{-6} for $p = 1, 2$ and $n = 20, 40, 80, 160$.

(a) $p = 1$

n	CG iterations	PCG iterations
20	45	24
40	89	25
80	174	27
160	341	28

(b) $p = 2$

n	CG iterations	PCG iterations
20	93	103
40	113	112
80	193	124
160	373	133

Example 5.2. Let $\hat{\Omega}$ be the same L-shaped domain and $\boldsymbol{G}$ the same geometry map as in Example 5.1, and

$$\begin{aligned} A(x_1, x_2) &= \begin{bmatrix} (2+\cos x_1)(1+x_2) & \cos(x_1+x_2)\sin(x_1+x_2) \\ \cos(x_1+x_2)\sin(x_1+x_2) & (2+\sin x_2)(1+x_1) \end{bmatrix}, \quad (x_1, x_2) \in \Omega, \\ \mathrm{f}(x_1, x_2) &= -\nabla \cdot A(x_1, x_2)\nabla u(x_1, x_2), \quad (x_1, x_2) \in \Omega, \\ \mathrm{g}(x_1, x_2) &= \cos(x_1 + 2x_2), \quad (x_1, x_2) \in \Gamma = \partial\Omega, \end{aligned}$$

where $u(x_1, x_2) = \cos(x_1 + 2x_2)$. We point again to Figure 5.1 for an illustration of the domains $\hat{\Omega}$ and Ω. The comparison between the eigenvalues of the matrix $L_{n,p}^{\boldsymbol{G},\mathrm{ext}}$ and the monotone rearrangement of the symbol $\mathbf{1}(|\det(J_{\boldsymbol{G}}(\hat{x}_1, \hat{x}_2))|A_{\boldsymbol{G}}(\hat{x}_1, \hat{x}_2) \circ H_{(p,p)}(\theta_1, \theta_2))\mathbf{1}^T$ is shown in Figure 5.3 for different values of p and even n. Some large eigenvalues (outliers) have been cut from the figures in order to allow for a better visualization of the matching between the other eigenvalues and the monotone rearrangement of the symbol. In Figure 5.4, we check the validity of the lower and upper bounds in (5.2) by showing the evaluations of both the symbol and its bounds on an equispaced grid in $\boldsymbol{G}^{-1}(\Omega) \times [-\pi, \pi]^2$ for different values of p. The comparison between the number of CG and PCG iterations for solving the linear system (3.4) up to a precision of 10^{-6} is shown in Table 5.2 for $p = 1, 2$ and different even values of n. We see that the number of PCG iterations is considerably lower than the number of CG iterations for $p = 1, 2$ and large n.

Example 5.3. Let $\hat{\Omega}$ be the pentagon with vertices $(0, 0)$, $(\frac{1}{2}, 0)$, $(1, \frac{1}{2})$, $(1, 1)$, $(0, 1)$, and

$$\begin{aligned} \boldsymbol{G}(\hat{x}_1, \hat{x}_2) &= \frac{1}{\sqrt{(1-\hat{x}_1)^2 + \hat{x}_2^2}} \begin{bmatrix} (1-\hat{x}_1)(1-\hat{x}_1+\hat{x}_2) \\ \hat{x}_2(1-\hat{x}_1+\hat{x}_2) \end{bmatrix}, \quad (\hat{x}_1, \hat{x}_2) \in \hat{\Omega}, \\ A(x_1, x_2) &= \begin{bmatrix} \mathrm{e}^{x_1 x_2} & \frac{x_1 x_2}{2} \\ \frac{x_1 x_2}{2} & \mathrm{e}^{x_1 + x_2} \end{bmatrix}, \quad (x_1, x_2) \in \Omega, \\ \mathrm{f}(x_1, x_2) &= -\nabla \cdot A(x_1, x_2)\nabla u(x_1, x_2), \quad (x_1, x_2) \in \Omega, \\ \mathrm{g}(x_1, x_2) &= \sin(2\pi x_1)\cos(\pi x_2), \quad (x_1, x_2) \in \Gamma = \partial\Omega, \end{aligned}$$

where $u(x_1, x_2) = \sin(2\pi x_1)\cos(\pi x_2)$. The domains $\hat{\Omega}$ and Ω are illustrated in Figure 5.5. The comparison between the eigenvalues of the matrix $L_{n,p}^{\boldsymbol{G},\mathrm{ext}}$ and the monotone rearrangement of the symbol $\mathbf{1}(|\det(J_{\boldsymbol{G}}(\hat{x}_1, \hat{x}_2))|A_{\boldsymbol{G}}(\hat{x}_1, \hat{x}_2) \circ H_{(p,p)}(\theta_1, \theta_2))\mathbf{1}^T$ is shown in Figure 5.6 for different values of p and even n. Some large eigenvalues (outliers) have been cut from the figures in order to allow for a better visualization of the matching between the other eigenvalues

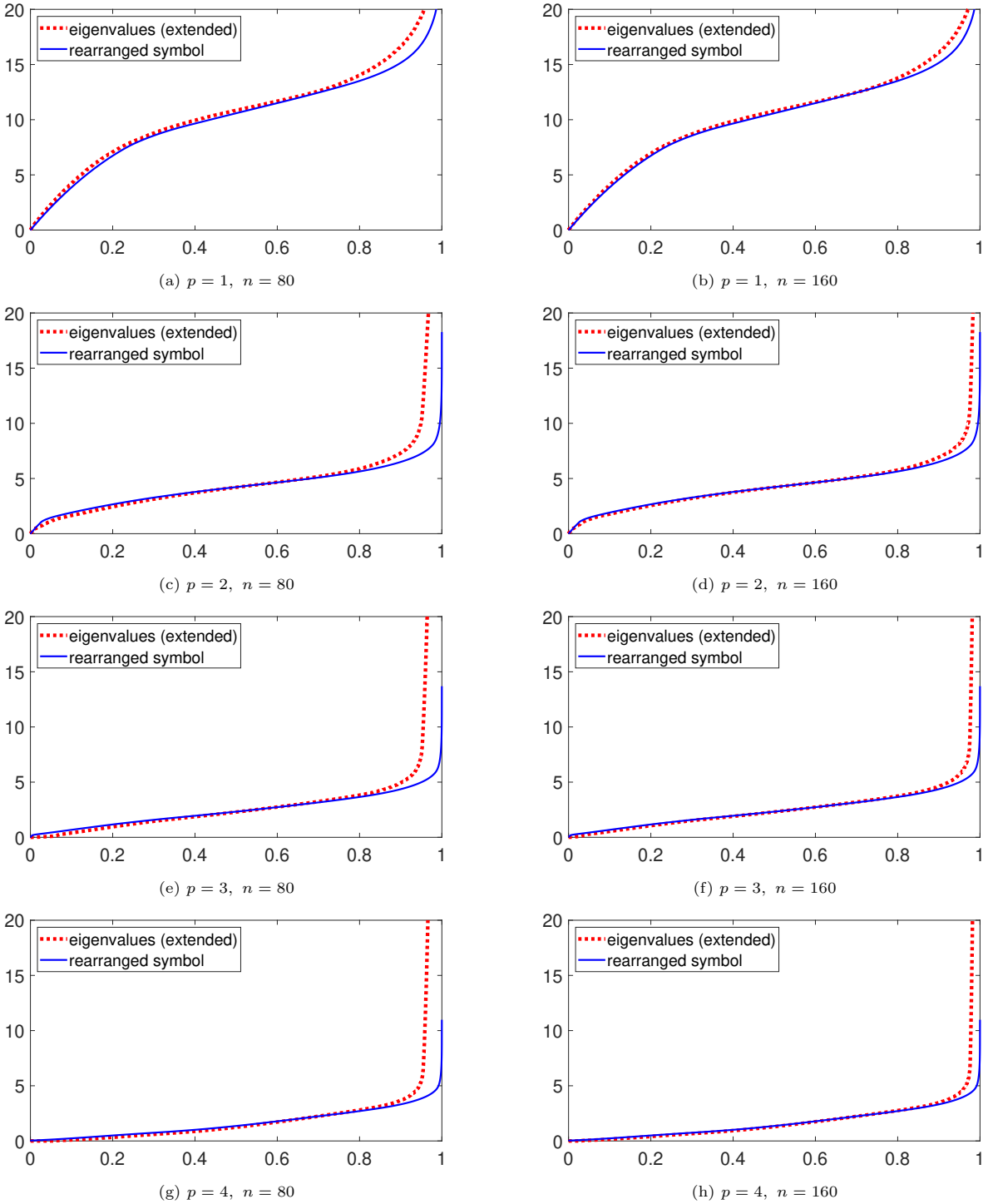

(a) $p = 1,\ n = 80$ (b) $p = 1,\ n = 160$

(c) $p = 2,\ n = 80$ (d) $p = 2,\ n = 160$

(e) $p = 3,\ n = 80$ (f) $p = 3,\ n = 160$

(g) $p = 4,\ n = 80$ (h) $p = 4,\ n = 160$

Figure 5.3: Example 5.2: Comparison between the eigenvalues of the matrix $L_{n,p}^{\boldsymbol{G},\text{ext}}$ (extended B-spline basis) and the monotone rearrangement of the symbol $\mathbf{1}(|\det(J_{\boldsymbol{G}}(\hat{x}_1,\hat{x}_2))|A_{\boldsymbol{G}}(\hat{x}_1,\hat{x}_2)\circ H_{(p,p)}(\theta_1,\theta_2))\mathbf{1}^T$ for $p = 1,2,3,4$ and $n = 80, 160$.

and the monotone rearrangement of the symbol. In Figure 5.7, we check the validity of the lower and upper bounds in (5.2) by showing the evaluations of both the symbol and its bounds on an equispaced grid in $\boldsymbol{G}^{-1}(\Omega)\times[-\pi,\pi]^2$ for different values of p. The comparison between the number of CG and PCG iterations for solving the linear system (3.4) up to a precision of 10^{-6} is shown in Table 5.3 for $p = 1,2$ and different even values of n. We see that the number of PCG iterations is considerably lower than the number of CG iterations for $p = 1,2$ and large n.

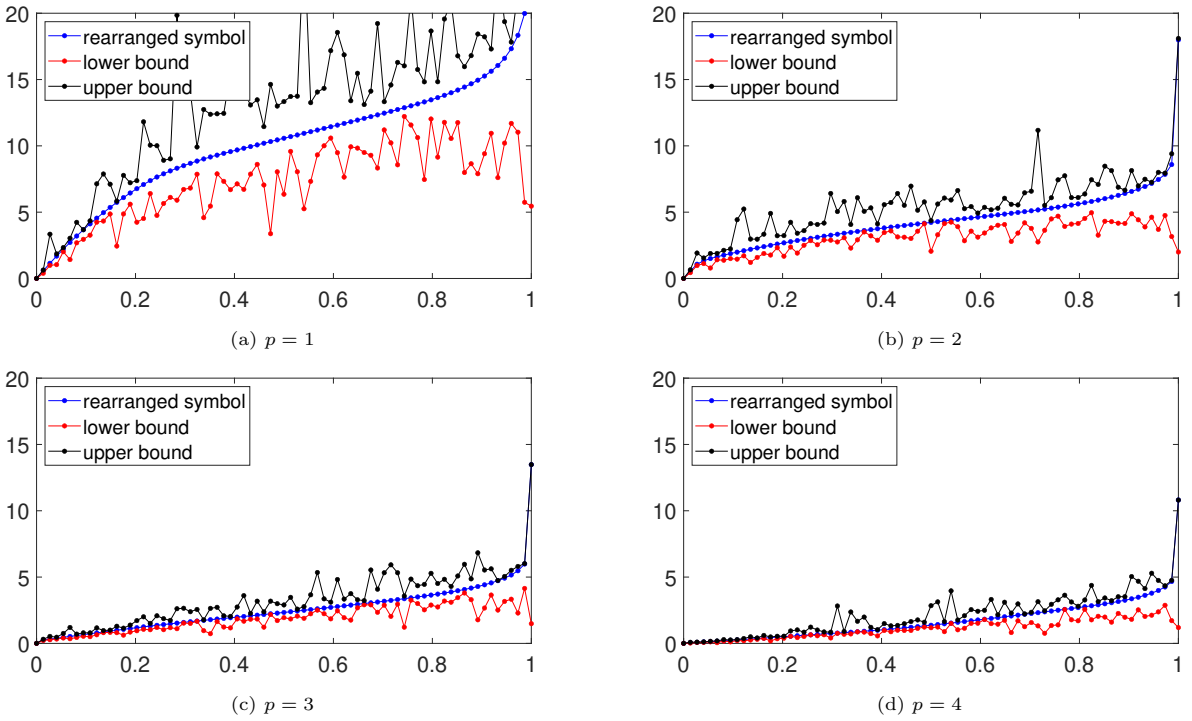

(a) $p = 1$ (b) $p = 2$

(c) $p = 3$ (d) $p = 4$

Figure 5.4: Example 5.2: Comparison between equispaced samples of the symbol $\mathbf{1}(|\det(J_{\boldsymbol{G}}(\hat{x}_1, \hat{x}_2))|A_{\boldsymbol{G}}(\hat{x}_1, \hat{x}_2) \circ H_{(p,p)}(\theta_1, \theta_2))\mathbf{1}^T$ and its bounds in (5.2) for $p = 1, 2, 3, 4$.

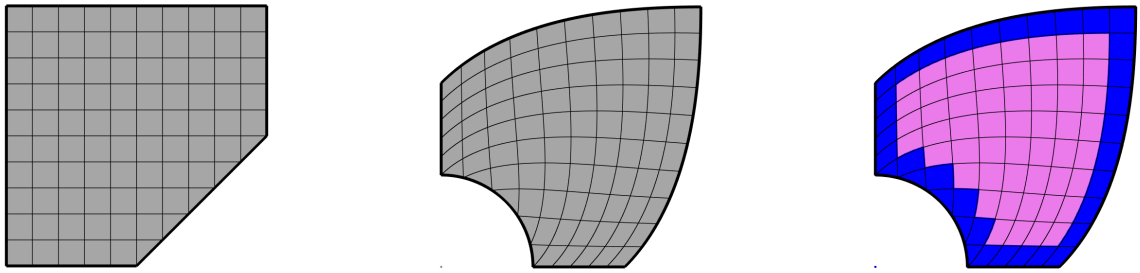

(a) $\hat{\Omega}$ (grey) (b) Ω (grey) (c) Ω_{in} (magenta) and $\Omega_{\Gamma,\text{in}}$ (blue)

Figure 5.5: Example 5.3: The parametric domain $\hat{\Omega}$, the physical domain Ω, and a possible mesh.

Table 5.3: Example 5.3: Number of CG and PCG iterations for solving the linear system (3.4) in the case of the extended B-spline basis up to a precision of 10^{-6} for $p = 1, 2$ and $n = 20, 40, 80, 160$.

(a) $p = 1$

n	CG iterations	PCG iterations
20	70	35
40	145	41
80	296	46
160	592	50

(b) $p = 2$

n	CG iterations	PCG iterations
20	113	114
40	156	148
80	315	170
160	638	194

6. Conclusions

We have considered immersed isogeometric discretizations for general Poisson problems with variable coefficients, where the physical domain Ω is described in terms of a trimmed geometry map $\boldsymbol{G}$, and we have analyzed the spectral

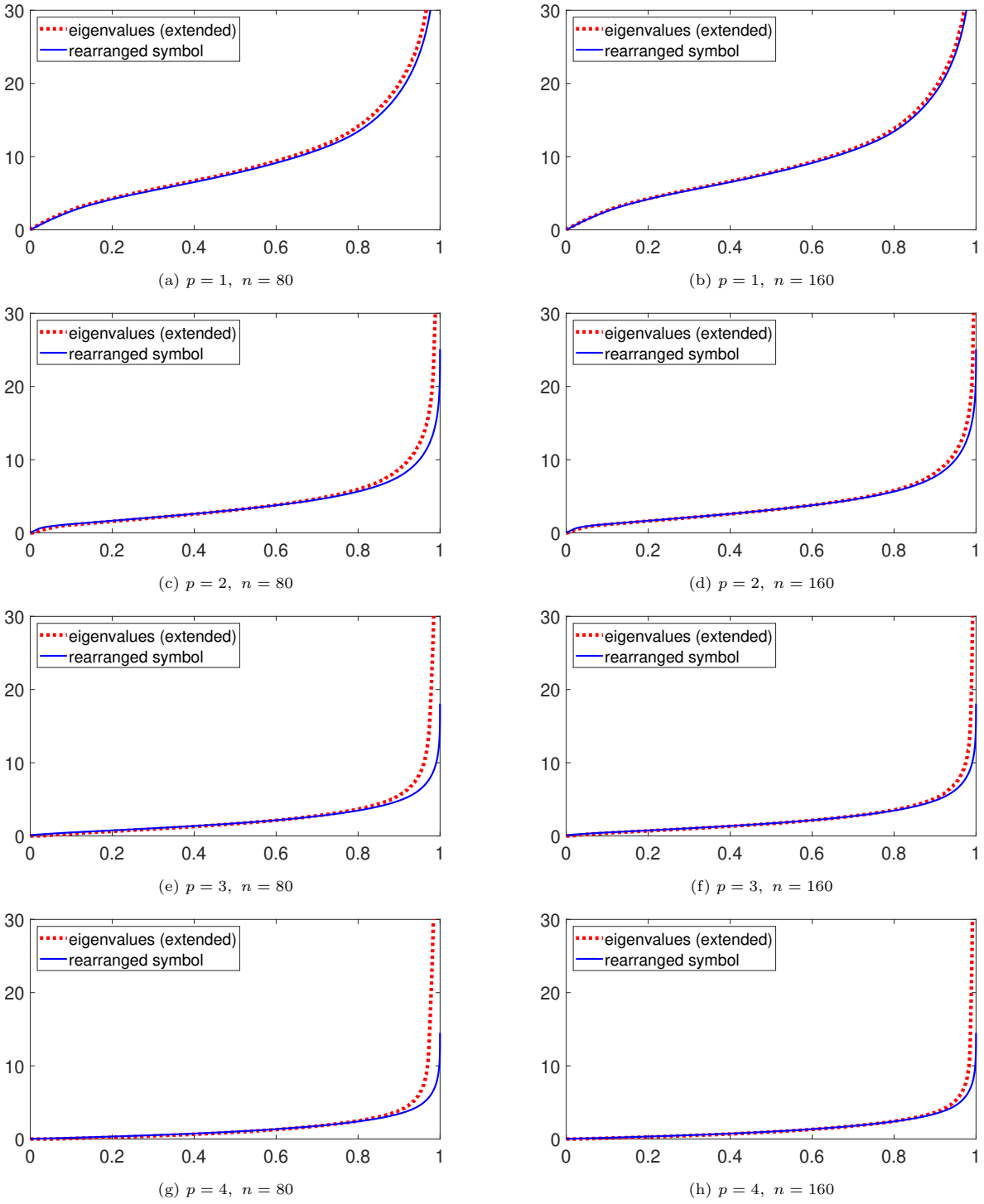

(a) $p = 1,\ n = 80$ (b) $p = 1,\ n = 160$

(c) $p = 2,\ n = 80$ (d) $p = 2,\ n = 160$

(e) $p = 3,\ n = 80$ (f) $p = 3,\ n = 160$

(g) $p = 4,\ n = 80$ (h) $p = 4,\ n = 160$

Figure 5.6: Example 5.3: Comparison between the eigenvalues of the matrix $L_{n,p}^{\boldsymbol{G},\text{ext}}$ (extended B-spline basis) and the monotone rearrangement of the symbol $\mathbf{1}(|\det(J_{\boldsymbol{G}}(\hat{x}_1,\hat{x}_2))|A_{\boldsymbol{G}}(\hat{x}_1,\hat{x}_2)\circ H_{(p,p)}(\theta_1,\theta_2))\mathbf{1}^T$ for $p = 1,2,3,4$ and $n = 80, 160$.

properties of the resulting (sequences of) matrices when the fineness of the discretization approaches zero, i.e., the size of the matrices goes to infinity.

In a complete analogy with the untrimmed case, the considered sequences of matrices enjoy an asymptotic spectral distribution described by a function called (spectral) symbol. This symbol does not depend on the boundary conditions but it incorporates the discretization technique, the geometry map, and the diffusion coefficients of the

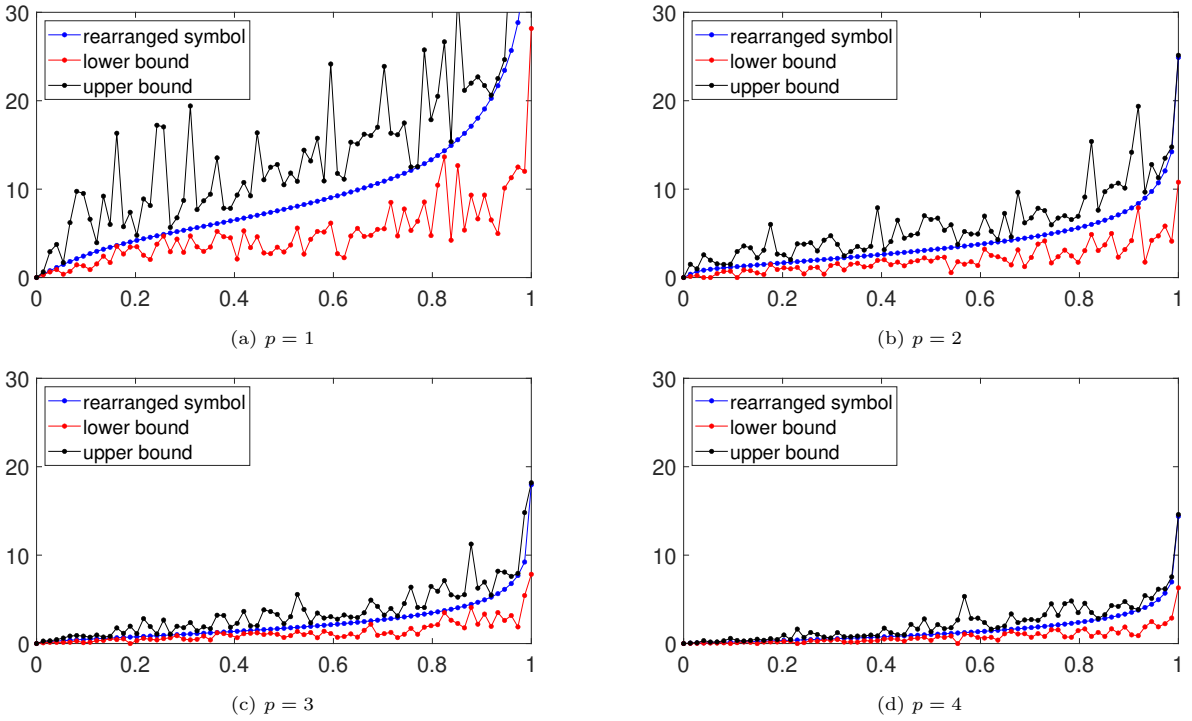

(a) $p = 1$ (b) $p = 2$

(c) $p = 3$ (d) $p = 4$

Figure 5.7: Example 5.3: Comparison between equispaced samples of the symbol $\mathbf{1}(|\det(J_{\boldsymbol{G}}(\hat{x}_1, \hat{x}_2))|A_{\boldsymbol{G}}(\hat{x}_1, \hat{x}_2) \circ H_{(p,p)}(\theta_1, \theta_2))\mathbf{1}^T$ and its bounds in (5.2) for $p = 1, 2, 3, 4$.

differential problem. Moreover, its structure and properties are completely analogous to the untrimmed case. The knowledge of the symbol and its properties allows us to identify potentially fast preconditioners for the considered matrices and we have proposed a specific CG preconditioner.

We have also presented a variety of numerical experiments illustrating both the performance of the proposed preconditioner and the fact that uniform samples of the (rearranged) symbol provide a good description of the exact eigenvalues of the considered matrices up to a small set of outliers, which are due to the low rank perturbation corresponding to the boundary conditions. The proposed preconditioner is particularly effective for low degrees. However, further investigation is advised for high degrees, which might require a deeper understanding of the behavior of the outliers.

As future work, a similar spectral analysis of immersed isogeometric discretizations could be carried out for other types of differential problems, e.g., the linear elasticity problem in [17]. It would also be interesting to apply the provided immersed framework to more complex geometries, e.g., the tunnel cross passage example in [23].

Acknowledgements

The authors are members of the research group GNCS (Gruppo Nazionale per il Calcolo Scientifico) of INdAM (Istituto Nazionale di Alta Matematica). This work has been supported by the MUR Excellence Department Project MatMod@TOV (CUP E83C23000330006) awarded to the Department of Mathematics of the University of Rome Tor Vergata, by the Department of Mathematics of the University of Rome Tor Vergata through the project RICH_GLT (CUP E83C22001650005), and by a GNCS project (CUP E53C22001930001).

References

[1] Baiges J., Codina R., Henke F., Shahmiri S., Wall W. A. *A symmetric method for weakly imposing Dirichlet boundary conditions in embedded finite element meshes.* Int. J. Numer. Methods Engrg. 90 (2012) 636–658.

[2] Barbarino G. *A systematic approach to reduced GLT.* BIT Numer. Math. 62 (2022) 681–743.

[3] Bertaccini D., Durastante F. *Iterative Methods and Preconditioning for Large and Sparse Linear Systems with Applications.* Taylor & Francis, Boca Raton (2018).

[4] Bhatia R. *Matrix Analysis.* Springer, New York (1997).

[5] de Boor C. *A Practical Guide to Splines.* Revised edition, Springer, New York (2001).

[6] Cottrell J. A., Hughes T. J. R., Bazilevs Y. *Isogeometric Analysis: Toward Integration of CAD and FEA.* Wiley, Chichester (2009).

[7] Donatelli M., Garoni C., Manni C., Serra-Capizzano S., Speleers H. *Spectral analysis and spectral symbol of matrices in isogeometric collocation methods.* Math. Comput. 85 (2016) 1639–1680.

[8] Donatelli M., Garoni C., Manni C., Serra-Capizzano S., Speleers H. *Symbol-based multigrid methods for Galerkin B-spline isogeometric analysis.* SIAM J. Numer. Anal. 55 (2017) 31–62.

[9] Garoni C., Manni C., Pelosi F., Serra-Capizzano S., Speleers H. *On the spectrum of stiffness matrices arising from isogeometric analysis.* Numer. Math. 127 (2014) 751–799.

[10] Garoni C., Manni C., Pelosi F., Speleers H. *Spectral analysis of matrices resulting from isogeometric immersed methods and trimmed geometries.* Comput. Methods Appl. Mech. Engrg. 400 (2022) 115551.

[11] Garoni C., Manni C., Serra-Capizzano S., Sesana D., Speleers H. *Spectral analysis and spectral symbol of matrices in isogeometric Galerkin methods.* Math. Comput. 86 (2017) 1343–1373.

[12] Garoni C., Manni C., Serra-Capizzano S., Sesana D., Speleers H. *Lusin theorem, GLT sequences and matrix computations: an application to the spectral analysis of PDE discretization matrices.* J. Math. Anal. Appl. 446 (2017) 365–382.

[13] Garoni C., Manni C., Serra-Capizzano S., Speleers H. *NURBS in isogeometric discretization methods: a spectral analysis.* Numer. Linear Algebra Appl. 27 (2020) e2318.

[14] Garoni C., Serra-Capizzano S. *Generalized Locally Toeplitz Sequences: Theory and Applications (Volume I).* Springer, Cham (2017).

[15] Garoni C., Serra-Capizzano S. *Generalized Locally Toeplitz Sequences: Theory and Applications (Volume II).* Springer, Cham (2018).

[16] Garoni C., Speleers H., Ekström S.-E., Reali A., Serra-Capizzano S., Hughes T. J. R. *Symbol-based analysis of finite element and isogeometric B-spline discretizations of eigevalue problems: exposition and review.* Arch. Comput. Methods Engrg. 26 (2019) 1639–1690.

[17] Giannelli C., Kanduč T., Pelosi F., Speleers H. *An immersed-isogeometric model: Application to linear elasticity and implementation with THBox-splines.* J. Comput. Appl. Math. 349 (2019) 410–423.

[18] Hardy Y., Steeb W.-H. *Matrix Calculus, Kronecker Product and Tensor Product: A Practical Approach to Linear Algebra, Multilinear Algebra and Tensor Calculus with Software Implementations.* 3rd ed., World Scientific, New Jersey (2019).

[19] Höllig K. *Finite Element Methods with B-Splines.* SIAM, Philadelphia (2003).

[20] Höllig K., Reif U., Wipper J. *Weighted extended B-spline approximation of Dirichlet problems.* SIAM J. Numer. Anal. 39 (2001) 442–462.

[21] Li Z., Ito K. *The Immersed Interface Method: Numerical Solutions of PDEs Involving Interfaces and Irregular Domains.* SIAM, Philadelphia (2006).

[22] Lyche T., Manni C., Speleers H. *Foundations of spline theory: B-splines, spline approximation, and hierarchical refinement.* In: Lyche T. et al. (eds.) Splines and PDEs: From Approximation Theory to Numerical Linear Algebra, Lect. Notes Math. 2219, pp. 1–76, Springer (2018).

[23] Marussig B., Hiemstra R., Hughes T. J. R. *Improved conditioning of isogeometric analysis matrices for trimmed geometries.* Comput. Methods Appl. Mech. Engrg. 334 (2018) 79–110.

[24] Marussig B., Hughes T. J. R. *A review of trimming in isogeometric analysis: challenges, data exchange and simulation aspects.* Arch. Comput. Methods Engrg. 25 (2018) 1059–1127.

[25] Pelosi F., Giannelli C., Manni C., Sampoli M. L., Speleers H. *Splines over regular triangulations in numerical simulation.* Comput. Aided Des. 82 (2017) 100–111.

[26] Serra-Capizzano S. *The GLT class as a generalized Fourier analysis and applications.* Linear Algebra Appl. 419 (2006) 180–233.

[27] Schillinger D., Dedè L., Scott M. A., Evans J. A., Borden M. J., Rank E., Hughes T. J. R. *An isogeometric design-through-analysis methodology based on adaptive hierarchical refinement of NURBS, immersed boundary methods, and T-spline CAD surfaces.* Comput. Methods Appl. Mech. Engrg. 249–252 (2012) 116–150.